Short Article

Cell Metabolism

Proteomics-Based Comparative Mapping of the Secretomes of Human Brown and White Adipocytes Reveals EPDR1 as a Novel Batokine

Graphical Abstract

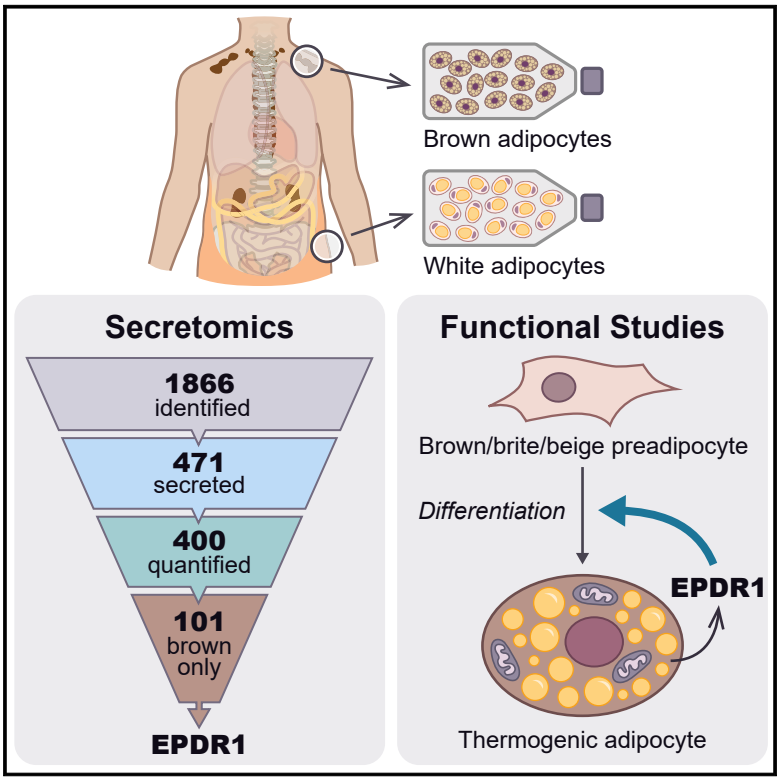

Authors

Atul S. Deshmukh, Lone Peijs, Jacqueline L. Beaudry, ..., Daniel J. Drucker, Matthias Mann, Camilla Scheele

Correspondence

matthias.mann@cpr.ku.dk (M.M.), cs@sund.ku.dk (C.S.)

In Brief

Deshmukh et al. describe the human brown fat secretome and identify novel candidate batokines with potential effects on human metabolism. One such batokine is EPDR1, shown here to play a role in brown fat commitment.

Highlights

- Identification of the first human brown fat secretome
- Comparative analysis of the secretomes of human brown and white adipocytes
- 101 proteins were exclusively identified in the secretome of brown adipocytes
- EPDR1 is a novel batokine important for brown fat commitment

Deshmukh et al., 2019, Cell Metabolism *30*, 1–13
November 5, 2019
https://doi.org/10.1016/j.cmet.2019.10.001

CellPress

Please cite this article in press as: Deshmukh et al., Proteomics-Based Comparative Mapping of the Secretomes of Human Brown and White Adipocytes Reveals EPDR1 as a Novel Batokine, Cell Metabolism (2019), https://doi.org/10.1016/j.cmet.2019.10.001

Cell Metabolism
Short Article

Proteomics-Based Comparative Mapping of the Secretomes of Human Brown and White Adipocytes Reveals EPDR1 as a Novel Batokine

Atul S. Deshmukh,[1,2,3,12] Lone Peijs,[3,4,12] Jacqueline L. Beaudry,[5] Naja Z. Jespersen,[4] Carsten H. Nielsen,[6,7] Tao Ma,[3] Andreas D. Brunner,[1] Therese J. Larsen,[4] Rafael Bayarri-Olmos,[8] Bhargav S. Prabhakar,[2] Charlotte Helgstrand,[9] Mai C.K. Severinsen,[4] Birgitte Holst,[10] Andreas Kjaer,[6] Mads Tang-Christensen,[9] Annika Sanfridson,[9] Peter Garred,[8] Gilbert G. Privé,[11] Bente K. Pedersen,[4] Zachary Gerhart-Hines,[3] Søren Nielsen,[4] Daniel J. Drucker,[5] Matthias Mann,[1,2,13,*] and Camilla Scheele[3,4,13,14,*]

[1]Department of Proteomics and Signal Transduction, Max-Planck-Institute of Biochemistry, Am Klopferspitz 18, 82152 Martinsried, Germany
[2]The Novo Nordisk Foundation Center for Protein Research, Faculty of Health and Medical Sciences, University of Copenhagen, Copenhagen 2200, Denmark
[3]Novo Nordisk Foundation Center for Basic Metabolic Research, Faculty of Health and Medical Sciences, University of Copenhagen, Copenhagen 2200, Denmark
[4]The Centre of Inflammation and Metabolism and the Centre for Physical Activity Research, Rigshospitalet, University of Copenhagen, Copenhagen 2100, Denmark
[5]The Lunenfeld-Tanenbaum Research Institute, Mt. Sinai Hospital, Department of Medicine, University of Toronto, Toronto, ON M5G 1X5, Canada
[6]Department of Clinical Physiology, Nuclear Medicine and PET and Cluster for Molecular Imaging, Department of Biomedical Sciences, Rigshospitalet and University of Copenhagen, Copenhagen 2200, Denmark
[7]Minerva Imaging ApS, Copenhagen 2200, Denmark
[8]Laboratory of Molecular Medicine, Department of Clinical Immunology, Rigshospitalet, University Hospital of Copenhagen, Copenhagen 2100, Denmark
[9]Global Drug Discovery, Novo Nordisk A/S, Måløv 2760, Denmark
[10]Department of Biomedical Sciences, Faculty of Health and Medical Sciences, University of Copenhagen, Copenhagen 2200, Denmark
[11]Princess Margaret Cancer Centre, Toronto, ON M5G 1L7, Canada
[12]These authors contributed equally
[13]Senior author
[14]Lead Contact
*Correspondence: matthias.mann@cpr.ku.dk (M.M.), cs@sund.ku.dk (C.S.)
https://doi.org/10.1016/j.cmet.2019.10.001

SUMMARY

Adipokines secreted from white adipose tissue play a role in metabolic crosstalk and homeostasis, whereas the brown adipose secretome is less explored. We performed high-sensitivity mass-spectrometry-based proteomics on the cell media of human adipocytes derived from the supraclavicular brown adipose and from the subcutaneous white adipose depots of adult humans. We identified 471 potentially secreted proteins covering interesting categories such as hormones, growth factors, extracellular matrix proteins, and proteins of the complement system, which were differentially regulated between brown and white adipocytes. A total of 101 proteins were exclusively quantified in brown adipocytes, and among these was ependymin-related protein 1 (EPDR1). EPDR1 was detected in human plasma, and functional studies suggested a role for EPDR1 in thermogenic determination during adipogenesis. In conclusion, we report substantial differences between the secretomes of brown and white human adipocytes and identify novel candidate batokines that can be important regulators of human metabolism.

Context and Significance

In this paper, researchers from the University of Copenhagen focused on identifying the entire spectrum (or "secretome") of proteins released by human white adipocytes and the heat-producing and energy-burning brown adipocytes. The authors found a substantial difference in the secretomes; for example, indicating a higher anti-inflammatory capacity in brown adipocytes and a higher ability of plasticity in white adipocytes. 101 proteins were exclusively quantified in the secretome of brown adipocytes. One of these proteins was EPDR1, which was found to be important for brown fat cell development. This study further provides a catalog of molecules that could be involved in regulating human metabolism, and possibly leading to the discovery of novel drug targets for obesity and its associated diseases.

INTRODUCTION

Adipose tissue is a major regulator of whole-body energy homeostasis by communication with the brain and other organs (Stern et al., 2016). Well-established mediators of adipocyte-derived crosstalk include leptin and adiponectin, which are produced and secreted by white adipose tissue (WAT) and contribute to the regulation of whole-body energy homeostasis (Ahima et al., 1996; Scherer et al., 1995). Adipokines derived from brown adipose tissue (BAT), known as batokines (Villarroya et al., 2017), are less investigated, especially in humans. BAT differs from WAT in its heat-producing capacity, providing an energy-consuming process, which is turned on or off in response to sympathetic activation (Cannon and Nedergaard, 2004). Considering the functional differences in WAT and BAT, batokines represent a poorly explored source of metabolic regulators. Some of the identified batokines have been described as having a hormonal function, enhancing BAT activity, improving glucose metabolism, or mediating browning of white fat (Lee et al., 2014; Stanford et al., 2013; Svensson et al., 2016). Batokines could also be represented by growth factors acting in an autocrine or paracrine manner by regulating BAT differentiation (Villarroya et al., 2017). Mapping of the human BAT secretome has previously been restricted by the lack of representative human BAT cell models as well as the challenges associated with measuring the secretome in cell culture media. However, the development of advanced secretomics technology as well as non-immortalized human BAT cell models has now made such experiments possible (Deshmukh et al., 2015; Jespersen et al., 2013; Meissner et al., 2013). In the current study, we investigate the secretomes of human brown and white adipocytes using high-resolution mass spectrometry (MS)-based proteomics. We mine the results for novel candidates with the potential for intercellular communication and perform follow up studies on Mammalian ependymin-related protein 1 (EPDR1), shown here to be a modulator of energy homeostasis and thermogenic commitment.

RESULTS AND DISCUSSION

The Secretome of Human Brown and White Adipocytes

Supraclavicular fat precursor cells (termed brown throughout this manuscript) were derived from five adult humans, as previously reported (Jespersen et al., 2013). The cell cultures were matched with subcutaneous fat precursor cells (termed white throughout this manuscript) with equal differentiation capacity as assessed by visual estimation of lipid droplet accumulation and expression of the adipocyte differentiation marker, fatty-acid-binding protein 4 (*FABP4*) (Figures 1A–1C). Mitochondrial uncoupling protein 1 (*UCP1*) was higher expressed in brown adipocytes, both at baseline (Figure 1D) and following stimulation with NE (Figure 1E). The robust *UCP1* expression underscores that these brown fat cell cultures represent an appropriate model for the subsequent secretome studies. We used high-resolution MS (Michalski et al., 2011) and automated computational analysis in MaxQuant (Cox and Mann, 2008) (Figure 1F), and detected 1,866 protein groups (protein entries that were distinguishable by MS of their identified peptides) in total in human brown and white adipocyte conditioned media (Figure 1G; Table S1). Of these, 471 were predicted to be secreted proteins, including 340 classically and 131 non-classically secreted proteins (Figure 1G; Table S1). Following our computational filtering for secreted proteins, the intracellular location protein category had decreased, whereas the categories related to protein secretion, such as glycoprotein, signal, and extracellular locations, were increased (Figure 1H). The intracellular protein portion was still high after the bioinformatics filtering for signal, secreted, and extracellular protein annotations. However, these proteins had "multiple annotations," and besides the intracellular annotation, they either had a signal peptide (72.5%) or had a second annotation as extracellular proteins (27.5%) (Figure 1H; Table S1). This is consistent with the idea that proteins may carry out different functions at different cellular locations (Huberts and van der Klei, 2010). Most of the secreted proteins were detected in cell culture media from both brown and white adipocytes (Figure 1G). However, vascular endothelial growth factor A (VEGF-A) was only identified in media from brown adipocytes, while leptin was exclusively identified in media from white adipocytes (Figure 1G; Table S1). This provides proof of concept as leptin is one of the most studied white fat-derived hormones (Stern et al., 2016), while VEGF-A is a growth factor previously reported as important for the development of functional BAT (Park et al., 2017; Shimizu et al., 2014). The presence of a signal peptide suggest secretion through the classical ER-Golgi pathway, yet hundreds of intracellular proteins are thought to be secreted through various non-classical pathways, including secretion from exosomes and microvesicles (Huberts and van der Klei, 2010; Nickel and Rabouille, 2009). Mapping of our dataset with Vesiclepedia (Kalra et al., 2012) and ExoCarta (Keerthikumar et al., 2016) revealed that almost all proteins overlapped with secreted proteins found in these two databases (Figure 1I).

Comparative Mapping of Human Brown versus White Adipocyte Secretomes

We applied label-free quantification based on the MaxLFQ algorithm, which has proven robust and allows a comparison of an arbitrary number of samples simultaneously (Cox et al., 2014). The secretomes were highly correlated within groups (median Pearson correlation for the brown adipocytes = 0.86; Figure 2A; Table S1).

The secretomes of brown and white adipocytes were sufficiently separated to classify them as distinct entities as visualized by a principal component analysis (PCA) (Figure 2B). In our search for novel batokines, we filtered for proteins that were annotated with gene ontologies (GOs) for growth factor activity or hormone activity. This identified six hormones (Figure 2C) and eight growth factors (Figure 2D; Table S2). We calculated the fold change for these proteins between unstimulated brown and white adipocytes (woNE brown/white), unstimulated and NE-stimulated brown adipocytes (brown NE/woNE), and unstimulated and NE-stimulated white adipocytes (white NE/woNE). Among the hormones was the well-described adipokine adiponectin (ADIPOQ) (Scherer et al., 1995; Stern et al., 2016) and Fibrillin-1 (FBN1), the precursor protein for the recently discovered adipose hormone asprosin (Duerrschmid et al., 2017; Romere et al., 2016). Among the growth factors, we observed that granulins (GRN) and hepatoma-derived growth factor

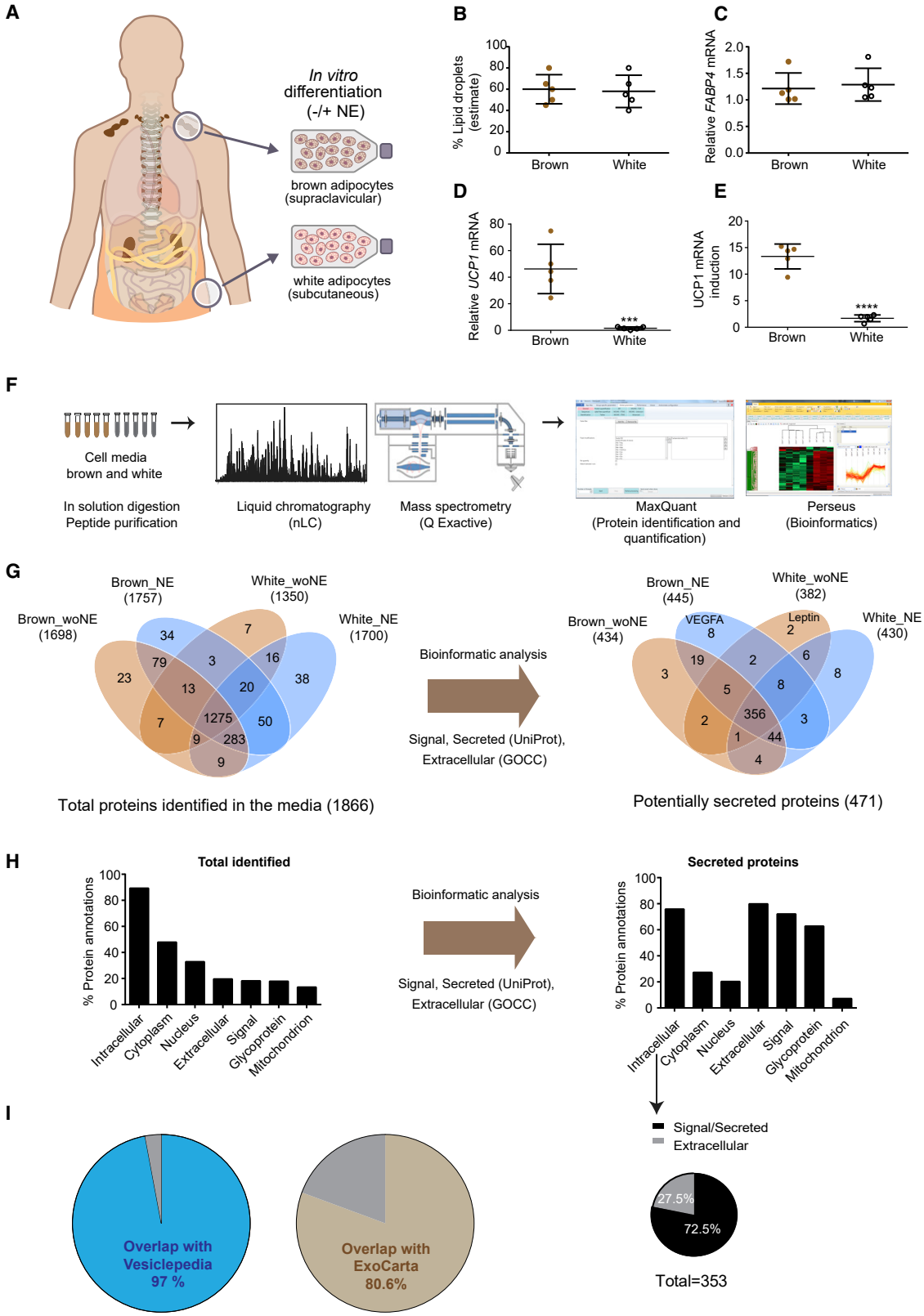

Figure 1. Model and Proteomics Workflow for Generating the Secretome of Human Brown and White Adipocytes

(A and B) (A) Mature adipocytes (brown adipocytes from n = 5 human donors; white adipocytes from n = 5 human donors) included in the study were characterized for (B) lipid droplet accumulation (estimated visually by phase contrast microscopy).

(legend continued on next page)

(HDGF) were more abundant in the brown adipocyte media than the white adipocyte media and could be considered as potential batokines. Granulins are cleaved into nine chains and have been described as autocrine growth factors important for wound healing (He et al., 2003). Granulins have not previously been described as batokines. However, one of the nine chains, acrogranin, also known as progranulin, was identified as a WAT-derived adipokine mediating high-fat diet (HFD)-induced insulin resistance in mice (Matsubara et al., 2012) and circulating levels of PRGN is associated with systemic insulin sensitivity in patients with metabolic syndrome (Li et al., 2014). HDGF promotes mitogenic activity through DNA-binding mediated transcriptional repression (Yang and Everett, 2007) but has also been detected in the extracellular region (Nüße et al., 2017). Taken together, our secretome analyses identified both established adipokines and novel candidate batokines and adipokines.

When comparing NE-induced secretomes in both brown and white adipocytes, we surprisingly observed many ribosomal proteins or proteins involved in translational processes (Table S2). We therefore decided to focus on the proteins secreted from brown and white adipocytes without norepinephrine stimulation in our search for novel batokines. A PCA plot including all proteins quantified under non-stimulated conditions revealed a clear separation between brown and white adipocytes (Figure 2E). A two-sample t test returned 143 differentially regulated proteins of which 106 were more abundant in cell media from brown adipocytes, while 37 were more abundant in cell media from white adipocytes (Figures 2F and 2G; Table S2). Fischer exact test (FDR = 0.02) for enrichment on significantly different protein in the background of total quantified proteins (1,113) returned only two categories: ''Extracellular (GOCC)'' and ''secreted (UniProt Keyword).'' This analysis suggests that the majority of differentially regulated proteins in brown and white adipocyte cell culture media are truly secreted proteins (Figure 2G). Several white-adipocyte-selective secreted proteins were extracellular matrix (ECM) associated, including transforming growth factor beta 1 (TGFB1), which has been associated with diabetes risk (Kim et al., 2013), and tenascin (TNC), an ECM glycoprotein with proinflammatory effects, which is highly expressed in WAT of obese patients and in murine models of obesity (Kim et al., 2013). We observed a more than 2-fold higher secretion of TNC and COL18A1 in cell media from white adipocytes compared to brown adipocytes. Cartilage intermediate layer protein 1 (CILP) and collagen alpha-1(XII) chain (COL12A1) were additional extracellular matrix proteins accumulating in the white adipocyte cell media (Figures 2G and 2H; Table S2). Interestingly, a recent comparative secretome study of murine interscapular brown and inguinal white adipocytes found that murine brown adipocytes secrete more ECM proteins (Ali Khan et al., 2018). These data suggest that the differences in ECM protein secretion might be either depot specific or species specific and provide a rationale for future investigations to understand the biological role of these secreted collagens and other ECM-associated proteins in the context of further defining the differences in WAT compared to BAT.

In brown adipocyte cell media, we detected highly abundant proteins with diverse functions. Parathymosin (PTMS) and prothymosin alpha (PTMA) were more than 4-fold more abundant in cell media from brown adipocytes than white adipocytes (Figure 2F). These relatively small proteins (11–12 kDa) were quantified with more than five unique peptides in cell media from brown adipocytes (Table S2) and have been shown to be involved in proliferation and regulation of immune function (Hannappel and Huff, 2003; Samara et al., 2017). The biological role of PTMS and PTMA in brown fat has not been explored. Although these proteins are not annotated as secreted, it is possible that they are secreted via exosomes or microvesicles from brown adipocytes. Interestingly, the clathrin-related proteins CLTA and CLTB, coating proteins of intracellular vesicles (Pearse, 1976), were also among the proteins with higher abundance in cell media from brown adipocytes compared to white adipocytes. This suggests that brown adipocytes make use of alternative secretion pathways such as vesicular trafficking more frequently than white adipocytes. Further, we observed that mitochondrial creatine kinase U-type (CKMT1) was more abundant in the media from brown adipocytes. This protein is involved in BAT mitochondrial energy metabolism (Kazak et al., 2015) and has gained interest as a human BAT-selective protein (Müller et al., 2016).

Among the proteins that were secreted in higher amounts from the brown adipocytes was a negative regulator of the innate immune system, complement factor H (CFH) (Figures 2F, 2I, and 2J). CFH inhibits the alternative pathway of the complement system by binding to C3b and enhancing the degradation of the alternative C3 convertase (C3bBb). In addition, CFH acts as a cofactor to complement factor I (CFI), a central inhibitor of all three complement system pathways, i.e., the classical, lectin, and alternative pathways (Zipfel and Skerka, 2009). Therefore, our MS data of the adipocyte media suggest that brown adipocytes might have higher anti-inflammatory capacity compared to white adipocytes. To verify our findings, we performed western blots on cell culture media from the brown and white adipocytes. In concordance, CFH immunoreactive protein was detected at relatively greater abundance in the media from brown adipocytes compared to white adipocytes (Figure 2K), and mRNA expression of *CFH* was higher in brown adipocytes versus white adipocytes (Figure 2L).

(C) *FABP4* mRNA expression.
(D) *UCP1* mRNA expression.
(E) *UCP1* mRNA induction, calculated as fold change between unstimulated and norepinephrine (NE) stimulated adipocytes (4 h stimulation).
Data in (B)–(E) are mean ± SEM; *p < 0.05, **p < 0.01, ***p < 0.001.
(F) Proteomics workflow.
(G) Overlap of the total amount of identified proteins between the different conditions, before and after filtering for proteins predicted to be secreted.
(H) Categorization of identified proteins before and after filtering for proteins predicted to be secreted.
(I) Overlap between identified secreted proteins and databases of secreted proteins; Vesiclepedia and ExoCarta.
See also Figure S1 and Table S1.

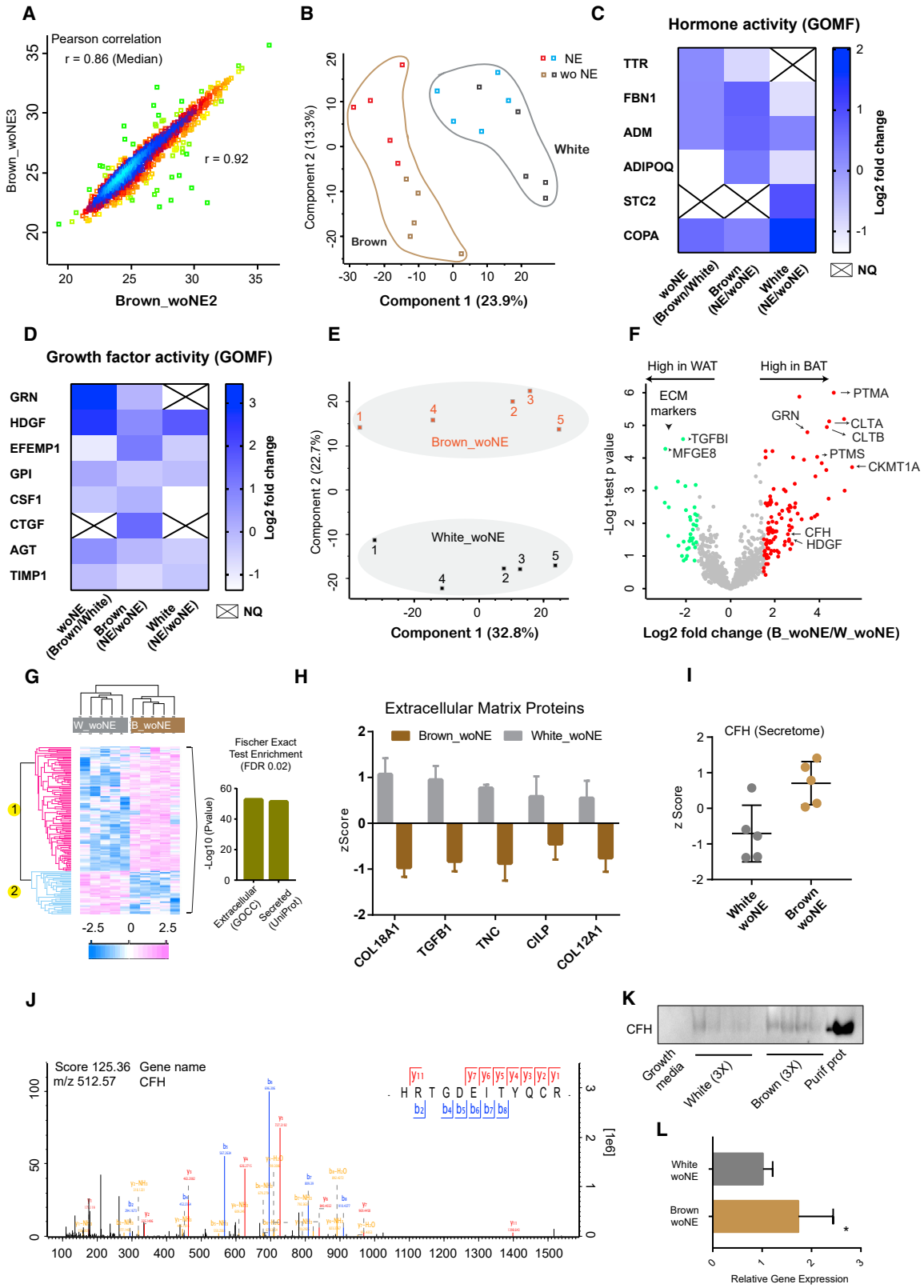

Figure 2. The Quantified Secretomes of Human Brown and White Adipocytes

(A) Representative Pearson correlation between two samples within the same group (brown adipocytes derived from two different individuals without NE stimulation).

(legend continued on next page)

A Distinct Secretome of Brown Adipocytes Identifies EPDR1 as a Candidate Batokine

Data-dependent quantitative proteomics data may contain a high percentage of missing values and systemic evaluation of the differentially expressed proteins is therefore important. For the comparative mapping described above, we imputed the missing values to best simulate the Gaussian distribution of low abundant proteins when comparing the secretomes of brown and white adipocytes, and we quantified more than 1,000 proteins expressed in cell media from both cell types, allowing for fold change comparison. However, we were concerned about the possibility that the imputation might mask differential regulation of low abundant proteins, even though the imputed values are downshifted. Thus, to avoid exclusion of any secreted protein that were selectively higher in the secretomes of either brown or white adipocytes, we investigated their selective secretomes separately. Using this approach, we exclusively quantified 101 proteins in the cell culture media from brown adipocytes, and 37 in the cell culture media from white adipocytes all these proteins were considered potentially secreted according to our criteria (Figure 3A; Table S2). Among the 101 proteins secreted from brown adipocytes was mammalian ependymin-related protein 1 (EPDR1) (Figure 3B). EPDR1 had previously been shortlisted in a TMT-labeling-based secretomics study of PR/SET domain 16 (PRDM16)-induced browning in mice (Svensson et al., 2016). We found EPDR1 to be exclusively quantified in BAT cell media (Figures S2A and S2B), while the imputation (Figure S2B) explains why EPDR1 was not annotated as differentially expressed in the volcano plot comparing the secretomes of white and brown adipocytes (Figure S2C). Consistent with these findings, *EPDR1* mRNA levels were higher in brown adipocytes compared to white adipocytes (Figure 3C). The *EPDR1* gene encodes three transcript variants, translated to three protein isoforms, of which two include an N-terminal signal peptide for secretion. We detected peptides unique to the secreted isoform 1, confirming its presence in our samples. Peptides mapping to isoform 2 (secreted) and isoform 3 (not secreted) were also detected, but these peptides also mapped to isoform 1; thus, their presence in our samples could be neither confirmed nor excluded (Figure 3D). These results do not exclude a low-level secretion of EPDR1 from white adipocytes. To further assess this, we performed a targeted proteomics of EPDR1. Notably, only one peptide could be quantified. Importantly, this peptide was unique to the secreted isoform 1, and the quantification confirmed that EPDR1 secretion is higher in cell media from brown adipocytes compared to media from white adipocytes (Figures S2D and S2E). We thus conclude that EPDR1 is selectively secreted from brown adipocytes yet also produced by white adipocytes, albeit likely in minimal amounts. Isoform 1 has been assigned as the canonical sequence, and as our data indicated that this isoform was detected in the brown adipocyte cell media, we decided to focus on this variant in our downstream experiments. As revealed by the crystal structure, EPDR1 has hydrophobic binding grooves and can interact with liposomes, suggesting a potential role in lipid transport (Wei et al., 2019).

To investigate the role of EPDR1 in brown adipocytes, we performed small interfering RNA (siRNA)-mediated knockdown. As the protein was expressed already at the onset of differentiation (Figure 3E), we transfected human brown adipocytes at day 0 of differentiation and measured *EPDR1* mRNA levels after 24 h and again after the full 12-day differentiation program. The siRNA knockdown was highly efficient and had a sustained effect throughout differentiation (Figure 3E). *EPDR1* mRNA levels were higher in the mature adipocytes than the early differentiation state (Figure 3E). The knockdown was also confirmed at the protein level (Figure S2F).

We observed no visual changes in lipid droplet accumulation or mitochondrial content following knockdown (Figure S2H). However, we found a decrease in the metabolic response to adrenergic signaling in brown adipocytes transfected with EPDR1 siRNA, as NE-induced proton leak was decreased (Figures 3F and 3G). In concordance, NE-induced upregulation of the thermogenic markers *DIO_2*, *UCP1*, *PPARGC1A*, *PPARα*, and *CKMT1* was blunted in these cells (Figure 3H). We validated these data using two additional siRNA oligos, also targeting *EPDR1*, and could reproduce the effects on *UCP1* regulation (Figure S2G). To further assess the effects of EPDR1 knockdown, we measured a range of thermogenic and adipogenic markers. Whereas many thermogenic and adipogenic markers remained unchanged following EPDR1 knockdown (Figures S2I and S2J), we found that the blunted thermogenic activation was accompanied by a reduced expression of GLUT4 (Figure 3I) and an increased expression of *COL1A2* and *PDGFRα*, suggesting a potential increase in an undifferentiated, fibroblastic state (Sun et al., 2017) (Figure 3J). Interestingly, *CITED1*, a beige fat marker (Sharp et al., 2012), was also increased (Figure 3J).

To further understand the metabolic deficiency in the cells differentiating with reduced amounts of EPDR1, we performed

(B) PCA plot, including all proteins quantified in brown and white adipocytes with (NE) and without NE (wo NE) stimulation.
(C) Quantified proteins in the datasets with hormone activity, as annotated with the gene ontology molecular function (GOMF) term. NQ, not quantified.
(D) Quantified proteins in the datasets with growth factor activity, identified with GOMF term.
(E) PCA plot, including all quantified proteins in unstimulated brown and white adipocytes.
(F) Volcano plot depicting a two-sample t test between all quantified proteins in unstimulated brown and white adipocytes.
(G) Heatmap of all differentially regulated proteins between unstimulated brown and white adipocytes, as determined by two-sample t test.
(H) ECM proteins in white adipopcytes compared to brown adipocytes.
(I) Secreted amounts of complement factor H (CFH). Values represent *Z* score from the mass spectrometry analysis of cell media.
Data in (B)–(I) are based on n = 5 brown adipocytes and n = 5 white adipocytes, biological replicates, all from separate human donors.
(J) Mass spectrometry trace of CFH.
(K) Western blot of CFH in brown and white adipocyte culture media from brown adipocyte cultures (n = 3) and white adipocyte cultures (n = 3); biological replicates, all from separate human donors.
(L) *CFH* relative mRNA levels in white (n = 5) and brown (n = 5) adipocytes, all derived from separate human donors. Data are mean ± SEM; $^{*}p < 0.05$, $^{**}p < 0.01$, $^{***}p < 0.001$.
See also Table S2.

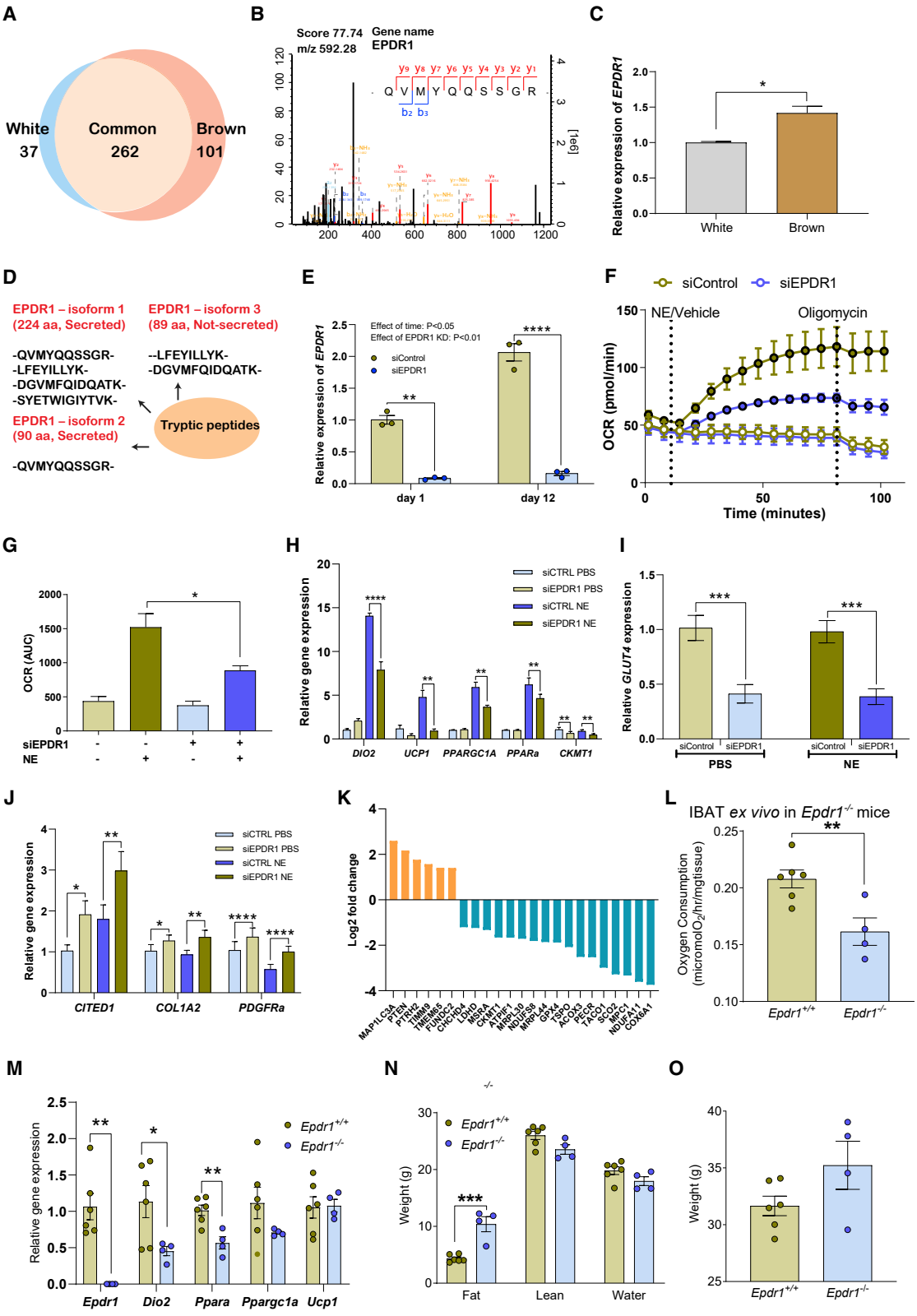

Figure 3. Identification and *In Vitro* Characterization of EPDR1, a Novel Batokine Candidate

(A) Venn diagram illustrating quantified proteins annotated as secreted.

(B) Example of EDPR1 unique peptides sequenced by mass spectrometry.

(legend continued on next page)

a cellular proteomics analysis on brown adipocytes derived from four human subjects and transfected at day 0 of differentiation with either siRNAs targeting EPDR1 or a non-targeting siRNA control. Cells were differentiated *in vitro* and harvested on day 12. We quantified 3,164 proteins in total of which 47 proteins were upregulated, and 53 proteins were downregulated following *EPDR1* knockdown (Table S3). Among the downregulated proteins were EPDR1 and GLUT4, consistent with our mRNA data (Table S3). To relate the proteomics data to the deficiency in NE- induced proton leak, we investigated whether mitochondria-associated proteins were among the regulated proteins. Indeed, the list of regulated proteins included 23 mitochondrial proteins (UniProt GO and Keywords annotation) of which 6 proteins were upregulated, whereas 17 were downregulated (Figure 3K). Among the downregulated molecular entities were key mitochondrial proteins, such as NDUFA11 and NDUFS8, core subunits of complex I in the mitochondrial respiratory chain; COX6A1, the terminal oxidase in mitochondrial electron transport; and CKMT1A, a key protein in creatine kinase-dependent thermogenesis (Kazak et al., 2015). Taken together, these data indicate that adipocytes lacking EPDR1 during differentiation exhibit a hampered mitochondrial phenotype, reducing the functional capacity of the mature brown adipocyte.

To further address this, we examined the status of interscapular brown fat (iBAT) in a previously uncharacterized Epdr1$^{-/-}$ whole-body knockout mouse. Interestingly, we found that *ex vivo* oxygen consumption was reduced in iBAT from Epdr1$^{-/-}$ compared to wild-type mice at 20 weeks of age (Figure 3L). This deficiency in thermogenic function was accompanied by a reduction in *Dio2* and *Pparα* mRNA levels in the *Epdr1*$^{-/-}$ mice compared to wild-type mice, whereas *Ucp1* and *Ppargc1a* mRNA levels remained unchanged (Figure 3M). Moreover, Epdr1$^{-/-}$ mice had a pronounced accumulation of body fat compared to control mice (Figure 3N), while total body weight was not different between groups (Figure 3O). These data, while encouraging, and directionally consistent with the totality of the EPDR1 data, should be interpreted with caution, as only a small number of mice were available for analysis and control mice were not littermates but were age- and gender-matched wild-type C57BL/6J.

Taken together, these data suggest that reduced levels of EPDR1 during differentiation results in incomplete brown fat commitment and thus propose a role for EPDR1 in thermogenic differentiation, perhaps as part of an auto- or paracrine circuit.

EPDR1 Affects Metabolism Independently of BAT Activity

Further characterization of the *Epdr1* whole-body knockout mouse revealed that at 9–11 weeks of age, the Epdr1$^{-/-}$ mice had a lower oxygen consumption than wild-type mice, which was mostly pronounced in the dark phase (Figure 4A). Interestingly, this was accompanied by a decrease in physical activity (Figure 4B) without differences in food intake (Figure 4C). These data suggested that the metabolic effects of mice lacking *Epdr1* in all tissues were not restricted to BAT.

To further investigate the effects of EPDR1 on whole-body metabolism, we produced recombinant EPDR1 (human isoform 1) (Figure S3A) and injected 14-week-old C57BL/6NRj mice with EPDR1 protein at 2 mg/kg. Mice were acclimatized to thermoneutrality prior to the injection, allowing us to assess whether EPDR1 had any effect on metabolism independently of cold stimulation. The injection was given just prior to the dark period, when BAT activity is naturally increased by murine circadian rhythm (Gerhart-Hines et al., 2013). Hence, we studied the effect of EPDR1 without cold stimulation but when BAT was metabolically primed. We recorded whole-body metabolism throughout the dark period using indirect calorimetry. Subcutaneous injection of EPDR1 protein resulted in an increase in oxygen consumption during a 12-h period as compared with control mice injected with PBS (Figure 4D). A corresponding increase in energy expenditure was observed, while respiratory exchange ratio (RER) remained unchanged (Figure S3B). Whereas no difference in locomotor activity was detected (Figure 4E), the increase in oxygen consumption was followed by a subsequent increase in food intake (Figure 4F), exemplifying the fine-tuned synergy between energy expenditure and energy intake (Contreras et al., 2014, 2017; Sutton et al., 2014). Based on the reduced

(C) EPDR1 isoform 1 mRNA expression in a representative white adipocyte culture (n = 3 independent experiments) and a representative brown adipocyte culture (n = 3 independent experiments).
(D) Tryptic peptides sequenced and mapped to EPDR1 isoforms.
For the downstream cell experiments in (E)–(J), a representative brown adipocyte culture was transfected with siRNAs (n=3 independent experiments).
(E) *EPRD1* mRNA expression at day 0 and at day 12 of differentiation, with and without knockdown of *EPDR1* (n = 3).
(F) Oxygen consumption rate in human brown adipocytes at day 12 of differentiation with or without *EPDR1* knockdown at day 0 and with or without NE stimulation (n = 3).
(G) Oxygen consumption rates following oligomycin treatment. The area under the curve for the three time points (88.09, 94.8, 101.47) following addition of oligomycin is presented for the four groups. An unpaired t test was performed to test differences between norepinephrine-stimulated leak in the siControl treated cells compared to the siEPDR1-treated cells.
(H) Relative mRNA expression of thermogenic markers *DIO_2*, *UCP1*, *PPARGC1A*, *PPARα*, and *CKMT1* (n = 3).
(I) Relative mRNA expression of *GLUT4* (n = 3).
(J) Relative mRNA expression of *CITED1*, *COL1A2*, and *PDGFRa*.
(K) Mitochondrial proteins differentially regulated in brown adipocytes at day 12 of differentiation following knockdown of EPDR1 at day 0 (n = 4 represents brown adipocytes derived from 4 different human donors).
(L) *Ex vivo* oxygen consumption in iBAT of Epdr1$^{-/-}$ mice (n = 4) and age-matched Epdr1$^{+/+}$ controls (n = 6).
(M) Relative mRNA expression of thermogenic markers *Dio2*, *Ucp1*, *Ppargc1a*, and *Pparα* in iBAT of *Epdr1*$^{-/-}$ mice (n = 4) and age-matched *Epdr1*$^{+/+}$ controls (n = 6).
(N) Weight of fat and lean mass in in iBAT of *Epdr1*$^{-/-}$ mice (n = 4) and age-matched *Epdr1*$^{+/+}$ controls (n = 6). Data are presented as mean ± SEM; *p < 0.5; **p < 0.01; ***p < 0.001; ****p < 0.0001.
See also Figure S2 and Table S2.

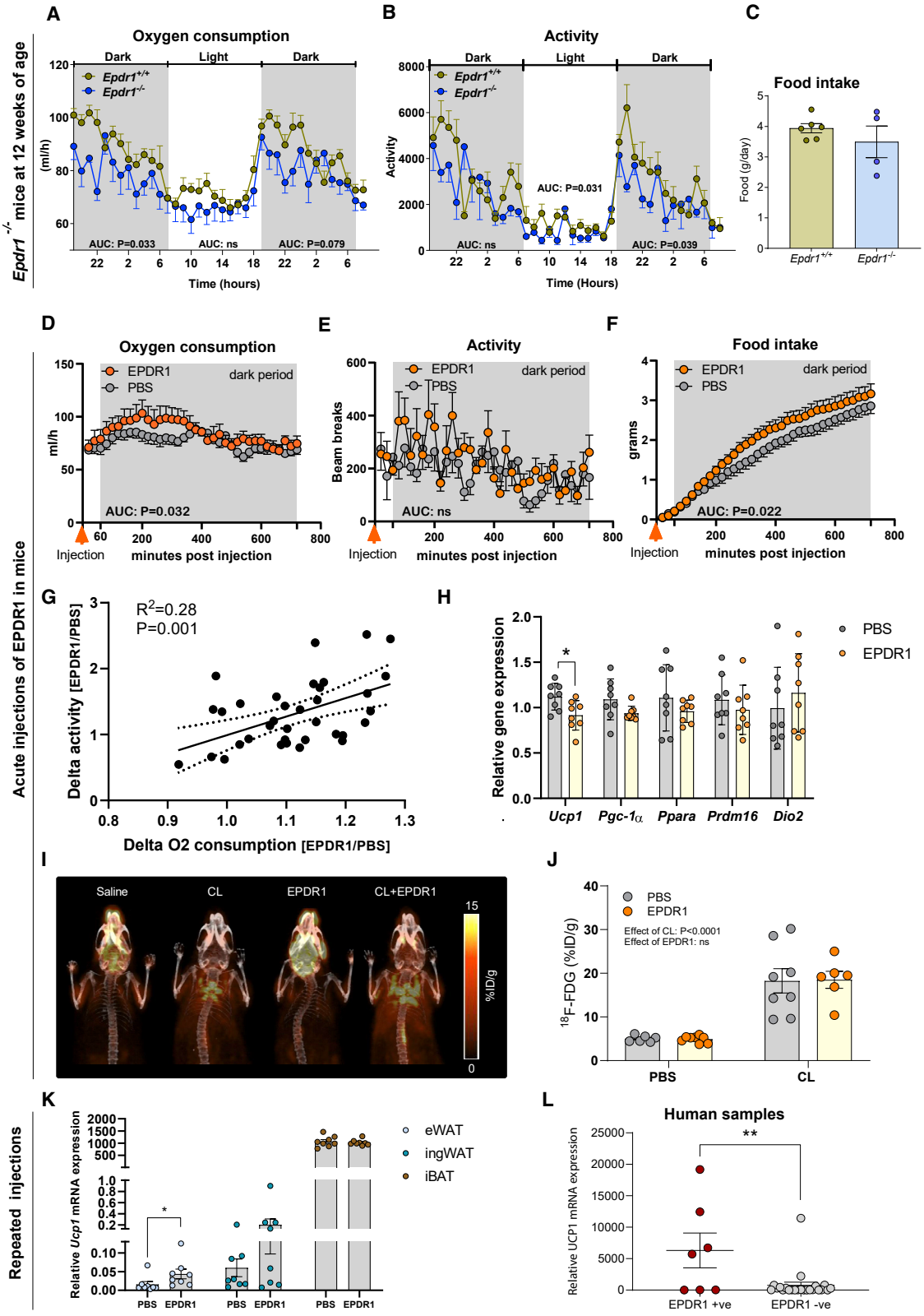

Figure 4. Effects of EPDR1 on Whole-Body Metabolism

(A) Oxygen consumption in *Epdr1*$^{-/-}$ (n = 4) or age-matched *Epdr1*$^{+/+}$ controls (n = 6).

(B) Locomotor activity in *Epdr1*$^{-/-}$ (n = 4) or age-matched *Epdr1*$^{+/+}$ controls (n = 6).

(legend continued on next page)

physical activity observed in the Epdr1$^{-/-}$ mice, we performed a linear regression analysis of the EPDR1-induced increases in oxygen consumption and physical activity, respectively. This revealed a correlation (R^2 = 0.28, p = 0.001), and the EPDR1-induced increase in oxygen consumption could thus at least partly be explained by elevated physical activity (Figure 4G). Consistent with this finding, we found no induction of genes linked to thermogenic activation (Figure 4H). In fact, we found a modest downregulation of *Ucp1*, while the rest of the markers were unchanged (Figure 4H).

Acute BAT activation in humans can be quantified by performing a PET/CT scan using a radioactive glucose tracer (Chen et al., 2016). This method can also be applied in anesthetized mice (Sustarsic et al., 2018). Although our data did not support that the increase in oxygen consumption was due to increased BAT activity, we decided to investigate this further using [18F] FDG-PET/CT scanning. Moreover, we aimed to assess whether a potential activation was interacting with a sympathetic tone. Therefore, we performed an experiment where EPDR1 was injected into C57BL/6NRj mice simultaneously with either PBS vehicle or the β3-agonist CL-316,243 (CL). Uptake of a glucose tracer ([18F] FDG) was then assessed by PET/CT in anesthetized animals. We observed a substantial increase in FDG uptake in mice that were injected with CL, but no further activity was detected with EPDR1 injections (Figures 4I and 4J). Consistent with the gene expression data obtained from the mice in the metabolic chambers, we observed a downregulation of *Ucp1*, and in this case, *Prdm16* was also reduced whereas other thermogenic markers including *Dio$_2$*, *Ppargc1a*, and *Pparα* remained unchanged (Figure S3C). In conclusion, EPDR1 affected metabolism but without enhancing BAT activity. Importantly, EPDR1 is expressed in other tissues, including the brain (Wei et al., 2019), possibly explaining the observed effects on metabolism.

To assess whether treatment with EPDR1 had any long-term effects on whole-body metabolism, we fed C57BL/6NRj mice a HFD and injected them with EPDR1 once daily for 21 days. We observed no difference in metabolic phenotype between the groups receiving EPDR1 compared to the group receiving PBS (Figure S3D). These mice were housed at room temperature, which is an appreciable cold stimulation and therefore could have masked EPDR1-dependent effects. Interestingly, we did observe an increase in *Ucp1* expression in WAT of mice that had been injected with EPDR1 protein (Figure 4K). Consistent with the lack of whole-body metabolic effects, the upregulation of *Ucp1* in the WAT following repeated injections of EPDR1 was very modest. This needs to be interpreted in the light of the mechanism of white fat browning. It has been reported that subpopulations of thermogenic adipocytes can be induced within epididymal (Petrovic et al., 2010) or inguinal (Seale et al., 2011) adipose tissues. It has further been demonstrated that thermogenic precursor cells co-exist with white fat precursor cells in the white fat depot (Wu et al., 2012). Therefore, measuring the whole tissue mRNA levels will likely dilute the upregulation of *Ucp1* limited to a thermogenic subpopulation. The reason that *Ucp1* expression in iBAT is not increased following the chronic stimulation is likely due to the room temperature housing conditions, which already result in efficient BAT recruitment (Sanchez-Gurmaches et al., 2018). Finally, we investigated whether EPDR1, as a secreted protein, could be detected in human plasma using a commercially available ELISA kit with a detection level of 30 ng/mL. We found that circulating EPDR1 was detected in seven out of thirty adult humans (Table S4). Interestingly, the subjects that were positive for EPDR1 had higher levels of *UCP1* mRNA in their deep neck brown adipose tissue, consistent with the possibility that EPDR1 could be secreted into the circulation perhaps from metabolically active BAT in humans (Figure 4L).

Collectively, we here provide the first comprehensive analysis of the human brown adipocyte secretome compared to the white adipocyte secretome in a basal state and following an acute NE stimulation. Our results reinforce that brown and white adipocytes have distinct secretory profiles and metabolic functions. We identify a large number of novel candidate batokines. Among several interesting candidates, we focused on the role of a novel human batokine, EPDR1, which is selectively secreted from brown adipocytes. We demonstrate that EPDR1 is vital for development into a functional thermogenic adipocyte, and our data further indicate that EPDR1 can act in an endocrine fashion. In conclusion, our data illuminate the human BAT secretome and provides a promising source of novel metabolic regulators that could serve as an important resource for future studies, including evaluation of potential drug targets for mediating improved metabolic control.

(C) Food intake in *Epdr1*$^{-/-}$ (n = 4) or age-matched *Epdr*$^{+/+}$ controls (n = 6).
(D) Oxygen consumption following EPDR1 protein (n = 8) or vehicle (n = 8) injection in C57Bl/6NRj mice at thermoneutrality (TN) during the dark period.
(E) Locomotor activity following EPDR1 (n = 8) or vehicle (n = 8) injection in C57Bl/6NRj mice at TN.
(F) Food intake following EPDR1 (n = 8) or vehicle (n = 8) injection in C57Bl/6NRj mice at TN.
(G) Linear regression analysis of the EPDR1-induced increases in oxygen consumption and physical activity.
(H) Relative mRNA expression of thermogenic markers in iBAT of C57/Bl/6NRj mice following EPDR1 (n = 8) or vehicle (n = 8) injection.
(I) Representative images of maximum intensity projection following injection of recombinant EPDR1 with and without injection of CL 316,243 at thermoneutrality and during FDG-PET/CT scanning (n = 6–8/group, as one mouse in the EPDR1-injected group was euthanized due to a paralyzed leg, and two mice in group in the EPDR1 + CL group were excluded due to bad injections).
(J) Quantification of maximum intensity in mice injected with or without recombinant EPDR1 and with and without CL 316,243 (n = 6–8 as described in I).
(K) Relative mRNA expression of *Ucp1* in eWAT, ingWAT, and iBAT of C57/Bl/6NRj mice on an HFD at room temperature following daily injections of EPDR1 or vehicle injections for 21 days (n = 8). The effects were tested using a two-way ANOVA, detecting an effect of tissue ($p < 0.0001$) and an effect of EPDR1 ($p < 0.05$). The tissue driving the effect of EPDR1 injections was further examined by using a Sidak's multiple comparisons test of which the p value is shown in the figure.
(L) EPDR1 protein levels were assessed in human plasma samples, and subjects were divided into two groups based on detectable levels (EPDR1+ve, n = 7) or no detection (EPDR1-ve, n = 23). An unpaired t test was used to assess differences. Relative gene expression of *UCP1* in deep neck surgical biopsies was measured using qPCR and plotted in the two groups. Data are presented as mean ± SEM; *$p < 0.5$; **$p < 0.01$; ***$p < 0.001$; ****$p < 0.0001$.
See also Figure S3.

Limitations of Study

Regarding the secretome analysis, methodological limitations could have resulted in that low abundant secreted proteins were not detected. Moreover, as we could exclude that some of the identified proteins originated from fragmented cells, we designed a computational pipeline to filter out proteins that were not likely to be secreted. This might, however, have resulted in removal of proteins that were secreted. On the other hand, we might have included proteins that were fragmentation products. Nevertheless, if any cell fragmentation had occurred, it is reasonable to expect that it occurred to the same extent between white and brown adipocytes as culturing and incubation conditions were identical. Our secretome analysis is done in mature adipocytes, but levels of (brown) adipokines differ during differentiation (Zhong et al., 2010). Analyses of more time points in the differentiation process could provide additional future insights into the secretory differences between white and brown adipocytes. We identify EPDR1 as a novel batokine, important for brown fat determination, whereas the exact pathway through which EPDR1 acts remains to be explored.

STAR★METHODS

Detailed methods are provided in the online version of this paper and include the following:

SUPPLEMENTAL INFORMATION

Supplemental Information can be found online at https://doi.org/10.1016/j.cmet.2019.10.001.

ACKNOWLEDGMENTS

We thank Jacob Steen Petersen and Birgitte Andersen from Novo Nordisk A/S for valuable scientific discussion, and Kirsten L. Meeske and Charlotte Wittrup from Minerva Imaging ApS for help with the scanning and data analysis. The Centre for Physical Activity Research (CFAS) is supported by TrygFonden (grant IDs 101390 and ID 20045). During the study period, the Center of Inflammation and Metabolism (CIM), Rigshospitalet, was supported by a grant from the Danish National Research Foundation (DNRF55). CIM/CFAS is a member of DD2, the Danish Center for Strategic Research in Type 2 Diabetes (the Danish Council for Strategic Research, grant nos. 09-067009 and 09-075724). Novo Nordisk Foundation Center for Basic Metabolic Research is an independent Research Center, based at the University of Copenhagen, Denmark, and partially funded by an unconditional donation from the Novo Nordisk Foundation (https://cbmr.ku.dk/) (grant no. NNF18CC0034900). Novo Nordisk Foundation Center for Protein Research (NNF14CC001) (https://www.cpr.ku.dk/) is supported by an unconditional grant from the Novo Nordisk Foundation to University of Copenhagen. M.M. was also supported by Max-Planck-Society for the Advancement of Science. D.J.D. was supported by a Banting and Best Diabetes Centre-Novo Nordisk Chair in Incretin Biology and CIHR operating grant 154321. Z.G.H. was supported by the European Research Council (ERC) under the European Union's Horizon 2020 Research and Innovation Programme (grant agreement no. 639382). N.Z.J. is supported by a research grant from the Danish Diabetes Academy, which is funded by the Novo Nordisk Foundation (grant no. NNF17SA0031406). P.G. and R.B.-O. were supported by the Danish Research Foundation of Independent Research (grant no. DFF-6110-00489). The study was further funded by a shared research grant from Novo Nordisk A/S to C.S. and M.M. and by a grant to C.S. from the Novo Nordisk Foundation (grant no. NNF18OC0034378).

AUTHOR CONTRIBUTIONS

C.S. and M.M. supervised the study. C.S., A.S.D., M.M., L.P., S.N., D.J.D., Z.-G.H., B.K.P., G.P., P.G., A.S., M.T.C., A.K., and B.H. performed hypothesis generation, conceptual design, data analysis, and manuscript preparation. L.P., A.S.D., J.L.B., N.Z.J., C.H.N., T.M., A.D.B., T.J.L., R.B-.O., B.S.P., C.H., and M.C.K.S. conducted experiments and data analysis. All authors edited and approved the final manuscript.

DECLARATION OF INTERESTS

D.J.D. has served as an advisor or consultant or speaker within the past 12 months to Forkhead Biotherapeutics, Heliome Inc., Intarcia Therapeutics, Kallyope, Merck Research Laboratories, Novo Nordisk Inc., Pfizer Inc., and Sanofi Inc. C.H., M.T.C., and A.S. are employees and shareholders at Novo Nordisk A/S. Z.G.H. works, in some capacity, for Embark Biotech Aps developing therapeutics for the treatment of diabetes and obesity.

Received: September 18, 2018
Revised: April 26, 2019
Accepted: October 2, 2019
Published: October 24, 2019

REFERENCES

Ahima, R.S., Prabakaran, D., Mantzoros, C., Qu, D., Lowell, B., Maratos-Flier, E., and Flier, J.S. (1996). Role of leptin in the neuroendocrine response to fasting. Nature *382*, 250–252.

Ali Khan, A., Hansson, J., Weber, P., Foehr, S., Krijgsveld, J., Herzig, S., and Scheideler, M. (2018). Comparative secretome analyses of primary murine white and brown adipocytes reveal novel adipokines. Mol. Cell. Proteomics *17*, 2357–2370.

Bradley, A., Anastassiadis, K., Ayadi, A., Battey, J.F., Bell, C., Birling, M.C., Bottomley, J., Brown, S.D., Bürger, A., Bult, C.J., et al. (2012). The mammalian gene function resource: the International Knockout Mouse Consortium. Mamm. Genome *23*, 580–586.

Cannon, B., and Nedergaard, J. (2004). Brown adipose tissue: function and physiological significance. Physiol. Rev. *84*, 277–359.

Chen, K.Y., Cypess, A.M., Laughlin, M.R., Haft, C.R., Hu, H.H., Bredella, M.A., Enerbäck, S., Kinahan, P.E., Lichtenbelt, Wv, Lin, F.I., et al. (2016). Brown adipose reporting criteria in imaging studies (BARCIST 1.0): recommendations for standardized FDG-PET/CT experiments in humans. Cell Metab. *24*, 210–222.

Contreras, C., Gonzalez, F., Fernø, J., Diéguez, C., Rahmouni, K., Nogueiras, R., and López, M. (2014). The brain and brown fat. Ann. Med. *47*, 150–168.

Contreras, C., Nogueiras, R., Diéguez, C., Rahmouni, K., and López, M. (2017). Traveling from the hypothalamus to the adipose tissue: the thermogenic pathway. Redox Biol. *12*, 854–863.

Cox, J., and Mann, M. (2008). MaxQuant enables high peptide identification rates, individualized p.p.b.-range mass accuracies and proteome-wide protein quantification. Nat. Biotechnol. *26*, 1367–1372.

Cox, J., Hein, M.Y., Luber, C.A., Paron, I., Nagaraj, N., and Mann, M. (2014). Accurate proteome-wide label-free quantification by delayed normalization and maximal peptide ratio extraction, termed MaxLFQ. Mol. Cell. Proteomics *13*, 2513–2526.

Deshmukh, A.S., Cox, J., Jensen, L.J., Meissner, F., and Mann, M. (2015). Secretome analysis of lipid-induced insulin resistance in skeletal muscle cells by a combined experimental and bioinformatics workflow. J. Proteome Res. *14*, 4885–4895.

Duerrschmid, C., He, Y., Wang, C., Li, C., Bournat, J.C., Romere, C., Saha, P.K., Lee, M.E., Phillips, K.J., Jain, M., et al. (2017). Asprosin is a centrally acting orexigenic hormone. Nat. Med. *23*, 1444–1453.

Gerhart-Hines, Z., Feng, D., Emmett, M.J., Everett, L.J., Loro, E., Briggs, E.R., Bugge, A., Hou, C., Ferrara, C., Seale, P., et al. (2013). The nuclear receptor Rev-erbα controls circadian thermogenic plasticity. Nature *503*, 410–413.

Hannappel, E., and Huff, T. (2003). The thymosins. Prothymosin alpha, parathymosin, and beta-thymosins: structure and function. Vitam. Horm. *66*, 257–296.

He, Z., Ong, C.H., Halper, J., and Bateman, A. (2003). Progranulin is a mediator of the wound response. Nat. Med. *9*, 225–229.

Huberts, D.H.E.W., and van der Klei, I.J. (2010). Moonlighting proteins: an intriguing mode of multitasking. Biochim. Biophys. Acta *1803*, 520–525.

Jespersen, N.Z., Larsen, T.J., Peijs, L., Daugaard, S., Homøe, P., Loft, A., De Jong, J., Mathur, N., Cannon, B., Nedergaard, J., et al. (2013). A classical brown adipose tissue mRNA signature partly overlaps with Brite in the supraclavicular region of adult humans. Cell Metab. *17*, 798–805.

Kalra, H., Simpson, R.J., Ji, H., Aikawa, E., Altevogt, P., Askenase, P., Bond, V.C., Borràs, F.E., Breakefield, X., Budnik, V., et al. (2012). Vesiclepedia: a compendium for extracellular vesicles with continuous community annotation. PLoS Biol. *10*, e1001450.

Kazak, L., Chouchani, E.T., Jedrychowski, M.P., Erickson, B.K., Shinoda, K., Cohen, P., Vetrivelan, R., Lu, G.Z., Laznik-Bogoslavski, D., Hasenfuss, S.C., et al. (2015). A creatine-driven substrate cycle enhances energy expenditure and thermogenesis in beige fat. Cell *163*, 643–655.

Keerthikumar, S., Chisanga, D., Ariyaratne, D., Al Saffar, H., Anand, S., Zhao, K., Samuel, M., Pathan, M., Jois, M., Chilamkurti, N., et al. (2016). ExoCarta: a web-based compendium of exosomal cargo. J. Mol. Biol. *428*, 688–692.

Kelstrup, C.D., Bekker-Jensen, D.B., Arrey, T.N., Hogrebe, A., Harder, A., and Olsen, J.V. (2018). Performance evaluation of the Q Exactive HF-X for shotgun proteomics. J. Proteome Res. *17*, 727–738.

Kim, Y., Kim, H.D., Youn, B., Park, Y.G., and Kim, J. (2013). Ribosomal protein S3 is secreted as a homodimer in cancer cells. Biochem. Biophys. Res. Commun. *441*, 805–808.

Kulak, N.A., Pichler, G., Paron, I., Nagaraj, N., and Mann, M. (2014). Minimal, encapsulated proteomic-sample processing applied to copy-number estimation in eukaryotic cells. Nat. Methods *11*, 319–324.

Larsen, T.J., Jespersen, N.Z., and Scheele, C. (2019). Adipogenesis in primary cell culture. In Handbook of Experimental Pharmacology (Springer), pp. 73–84.

Lee, P., Linderman, J.D., Smith, S., Brychta, R.J., Wang, J., Idelson, C., Perron, R.M., Werner, C.D., Phan, G.Q., Kammula, U.S., et al. (2014). Irisin and FGF21 are cold-induced endocrine activators of brown fat function in humans. Cell Metab. *19*, 302–309.

Li, H., Zhou, B., Xu, L., Liu, J., Zang, W., Wu, S., and Sun, H. (2014). Circulating PGRN is significantly associated with systemic insulin sensitivity and autophagic activity in metabolic syndrome. Endocrinology *155*, 3493–3507.

Matsubara, T., Mita, A., Minami, K., Hosooka, T., Kitazawa, S., Takahashi, K., Tamori, Y., Yokoi, N., Watanabe, M., Matsuo, E., et al. (2012). PGRN is a key adipokine mediating high fat diet-induced insulin resistance and obesity through IL-6 in adipose tissue. Cell Metab. *15*, 38–50.

Meissner, F., Scheltema, R.A., Mollenkopf, H.J., and Mann, M. (2013). Direct proteomic quantification of the secretome of activated immune cells. Science *340*, 475–478.

Michalski, A., Damoc, E., Hauschild, J.P., Lange, O., Wieghaus, A., Makarov, A., Nagaraj, N., Cox, J., Mann, M., and Horning, S. (2011). Mass spectrometry-based proteomics using Q Exactive, a high-performance benchtop Quadrupole Orbitrap Mass Spectrometer. Mol. Cell. Proteomics *10*, M111.011015.

Müller, S., Balaz, M., Stefanicka, P., Varga, L., Amri, E.Z., Ukropec, J., Wollscheid, B., and Wolfrum, C. (2016). Proteomic analysis of human brown adipose tissue reveals utilization of coupled and uncoupled energy expenditure pathways. Sci. Rep. *6*, 30030.

Nickel, W., and Rabouille, C. (2009). Mechanisms of regulated unconventional protein secretion. Nat. Rev. Mol. Cell Biol. *10*, 148–155.

Nüße, J., Blumrich, E.M., Mirastschijski, U., Kappelmann, L., Kelm, S., and Dietz, F. (2017). Intra- or extra-exosomal secretion of HDGF isoforms: the extraordinary function of the HDGF-A N-terminal peptide. Biol. Chem. *398*, 793–811.

Park, J., Kim, M., Sun, K., An, Y.A., Gu, X., and Scherer, P.E. (2017). VEGF-A - expressing adipose tissue shows rapid beiging and enhanced survival after transplantation and confers IL-4-independent metabolic improvements. Diabetes *66*, 1479–1490.

Pearse, B.M.F. (1976). Clathrin: a unique protein associated with intracellualar transfer of membrane by coated vesicles. Proc. Natl. Acad. Sci. USA *73*, 1255–1259.

Perez-Riverol, Y., Csordas, A., Bai, J., Bernal-Llinares, M., Hewapathirana, S., Kundu, D.J., Inuganti, A., Griss, J., Mayer, G., Eisenacher, M., et al. (2019). The PRIDE database and related tools and resources in 2019: improving support for quantification data. Nucleic Acids Res. *47*, D442–D450.

Petrovic, N., Walden, T.B., Shabalina, I.G., Timmons, J.A., Cannon, B., and Nedergaard, J. (2010). Chronic peroxisome proliferator-activated receptor gamma (PPARG) activation of epididymally derived white adipocyte cultures reveals a population of thermogenically competent, UCP1-containing adipocytes molecularly distinct from classic brown adipocytes. J. Biol. Chem. *285*, 7153–7164.

Romere, C., Duerrschmid, C., Bournat, J., Constable, P., Jain, M., Xia, F., Saha, P.K., Del Solar, M., Zhu, B., York, B., et al. (2016). Asprosin, a fasting-induced glucogenic protein hormone. Cell *165*, 566–579.

Samara, P., Karachaliou, C.E., Ioannou, K., Papaioannou, N.E., Voutsas, I.F., Zikos, C., Pirmettis, I., Papadopoulos, M., Kalbacher, H., Livaniou, E., et al. (2017). Prothymosin alpha: an Alarmin and more. Curr. Med. Chem. *24*, 1747–1760.

Sanchez-Gurmaches, J., Tang, Y., Jespersen, N.Z., Wallace, M., Martinez Calejman, C., Gujja, S., Li, H., Edwards, Y.J.K., Wolfrum, C., Metallo, C.M., et al. (2018). Brown fat AKT2 is a cold-induced kinase that stimulates ChREBP-mediated de novo lipogenesis to optimize fuel storage and thermogenesis. Cell Metab. *27*, 195–209.e6.

Scheltema, R.A., and Mann, M. (2012). SprayQc: a real-time LC-MS/MS quality monitoring system to maximize uptime using off the shelf components. J. Proteome Res. *11*, 3458–3466.

Scherer, P.E., Williams, S., Fogliano, M., Baldini, G., and Lodish, H.F. (1995). A novel serum protein similar to C1q, produced exclusively in adipocytes. J. Biol. Chem. *270*, 26746–26749.

Seale, P., Conroe, H.M., Estall, J., Kajimura, S., Frontini, A., Ishibashi, J., Cohen, P., Cinti, S., and Spiegelman, B.M. (2011). Prdm16 determines the thermogenic program of subcutaneous white adipose tissue in mice. J. Clin. Invest. *121*, 96–105.

Sharp, L.Z., Shinoda, K., Ohno, H., Scheel, D.W., Tomoda, E., Ruiz, L., Hu, H., Wang, L., Pavlova, Z., Gilsanz, V., et al. (2012). Human BAT possesses molecular signatures that resemble beige/Brite cells. PLoS One *7*, e49452.

Shimizu, I., Aprahamian, T., Kikuchi, R., Shimizu, A., Papanicolaou, K.N., MacLauchlan, S., Maruyama, S., and Walsh, K. (2014). Vascular rarefaction mediates whitening of brown fat in obesity. J. Clin. Invest. *124*, 2099–2112.

Stanford, K.I., Middelbeek, R.J., Townsend, K.L., An, D., Nygaard, E.B., Hitchcox, K.M., Markan, K.R., Nakano, K., Hirshman, M.F., Tseng, Y.H., et al. (2013). Brown adipose tissue regulates glucose homeostasis and insulin sensitivity. J. Clin. Invest. *123*, 215–223.

Stern, J.H., Rutkowski, J.M., and Scherer, P.E. (2016). Adiponectin, leptin, and fatty acids in the maintenance of metabolic homeostasis through adipose tissue crosstalk. Cell Metab. *23*, 770–784.

Sun, C., Berry, W.L., and Olson, L.E. (2017). PDGFRα controls the balance of stromal and adipogenic cells during adipose tissue organogenesis. Development *144*, 83–94.

Sustarsic, E.G., Ma, T., Lynes, M.D., Larsen, M., Karavaeva, I., Havelund, J.F., Nielsen, C.H., Jedrychowski, M.P., Moreno-Torres, M., Lundh, M., et al. (2018). Cardiolipin synthesis in brown and beige fat mitochondria is essential for systemic energy homeostasis. Cell Metab. *28*, 159–174.e11.

Sutton, A.K., Pei, H., Burnett, K.H., Myers, M.G., Rhodes, C.J., and Olson, D.P. (2014). Control of food intake and energy expenditure by Nos1 neurons of the paraventricular hypothalamus. J. Neurosci. *34*, 15306–15318.

Svensson, K.J., Long, J.Z., Jedrychowski, M.P., Cohen, P., Lo, J.C., Serag, S., Kir, S., Shinoda, K., Tartaglia, J.A., Rao, R.R., et al. (2016). A secreted slit2 fragment regulates adipose tissue thermogenesis and metabolic function. Cell Metab. *23*, 454–466.

Tyanova, S., Temu, T., Sinitcyn, P., Carlson, A., Hein, M.Y., Geiger, T., Mann, M., and Cox, J. (2016). The Perseus computational platform for comprehensive analysis of (prote)omics data. Nat. Methods *13*, 731–740.

Villarroya, F., Cereijo, R., Villarroya, J., and Giralt, M. (2017). Brown adipose tissue as a secretory organ. Nat. Rev. Endocrinol. *13*, 26–35.

Wei, Y., Xiong, Z.J., Li, J., Zou, C., Cairo, C.W., Klassen, J.S., and Privé, G.G. (2019). Crystal structures of human lysosomal EPDR1 reveal homology with the superfamily of bacterial lipoprotein transporters. Commun. Biol. *2*, 52.

Wu, J., Boström, P., Sparks, L.M.M., Ye, L., Choi, J.H.H., Giang, A.-H.H., Khandekar, M., Virtanen, K.A.A., Nuutila, P., Schaart, G., et al. (2012). Beige adipocytes are a distinct type of thermogenic fat cell in mouse and human. Cell *150*, 366–376.

Yang, J., and Everett, A.D. (2007). Hepatoma derived growth factor binds DNA through the N-terminal PWWP domain. BMC Mol. Biol. *8*, 101.

Zhong, J., Krawczyk, S.A., Chaerkady, R., Huang, H., Goel, R., Bader, J.S., Wong, G.W., Corkey, B.E., and Pandey, A. (2010). Temporal profiling of the secretome during adipogenesis in humans. J. Proteome Res. *9*, 5228–5238.

Zipfel, P.F., and Skerka, C. (2009). Complement regulators and inhibitory proteins. Nat. Rev. Immunol. *9*, 729–740.

STAR★METHODS

KEY RESOURCES TABLE

REAGENT or RESOURCE	SOURCE	IDENTIFIER
Antibodies		
Rabbit Polyclonal anti-UCC1 (EPDR1), 1:1000	Thermo Fisher Scientific	Cat#PA5-50404; RRID: AB_2635857
Mouse Monoclonal anti-α-Tubulin (clone DM1A), 1:1000	Sigma-Aldrich (Merck)	Cat#T9026; RRID: AB_477593
Mouse polyclonal anti-CFH, 1.8 μg/ml	This paper	N/A
Biological Samples		
Human supraclavicular brown adipocytes and subcutaneous white adipocytes	Jespersen et al., 2013	N/A
Human supraclavicular brown adipose tissue	This paper	N/A
Human plasma samples	This paper	N/A
Chemicals, Peptides, and Recombinant Proteins		
Seahorse XF base medium	Agilent	Cat#103335-100
FGF-1	Immunotools	Cat# 11343557
Transferrin	Sigma-Aldrich (Merck)	Cat#T8158
T3	Sigma-Aldrich (Merck)	Cat#T5516
Rosiglitazone	Sigma-Aldrich (Merck)	Cat#R2408
Dexamethazone	Sigma-Aldrich (Merck)	Cat#D4902
IBMX	Sigma-Aldrich (Merck)	Cat#I5879
DMEM/F-12, HEPES, no phenol red	Thermo Fisher Scientific	Cat#11039-047
FBS	Thermo Fisher Scientific	Cat#10270106
Opti-MEM I Reduced Serum Medium	Thermo Fisher Scientific	Cat#31985062
Lipofectamine RNAiMAX Transfection Reagent	Thermo Fisher Scientific	Cat#13778150
Sodium pyruvate	Sigma-Aldrich (Merck)	Cat#5280
L-Glutamine	Sigma-Aldrich (Merck)	Cat#G5126
D-(+) Glucose	Sigma-Aldrich (Merck)	Cat#G7021
MitoTracker Red CMXRos	Thermo Fisher Scientific	Cat#M7512
NucBlue Fixed Cell ReadyProbes Reagent	Thermo Fisher Scientific	Cat#R37606
PBS, pH 7.4	Thermo Fisher Scientific	Cat#10010049
PowerUp SYBR Green Master Mix	Thermo Fisher Scientific	Cat#A25777
TaqMan Universal PCR Master Mix	Thermo Fisher Scientific	Cat#4305719
BODIPY 493/503	Thermo Fisher Scientific	Cat#D-3922
NORadrenalin SAD	Amgros I/S	Cat#745661
Insulin (Actrapid)	Novo Nordisk	Cat#A10AB01
EPDR1 protein	Novo Nordisk	N/A
High fat diet for rodents with lard (60% kJ fat)	Ssniff	D12495
Critical Commercial Assays		
High-Capacity cDNA Reverse Transcription kit	Thermo Fisher Scientific	Cat#4374966
Direct-zol RNA miniprep kit	Zymo Research	Cat#R2063
Seahorse XFe96 FluxPak	Agilent	Cat#102416-100
EPDR1 ELISA kit	MyBioSource	Cat#MBS9316185
Seahorse XF Cell Mito Stress Test Kit	Agilent	Cat#103015-100
Bio-Rad Protein Assay	Bio-Rad	Cat#5000006
Deposited Data		
Raw and processed MS data	ProteomeXchange Consortium	ProteomeXchange: PXD008541

(*Continued on next page*)

Continued

REAGENT or RESOURCE	SOURCE	IDENTIFIER
Experimental Models: Organisms/Strains		
Mouse: Male wild-type C57Bl/6NRj	Janvier	N/A
Mouse: Female C57Bl/6NRj	Janvier	N/A
Mouse: Male *Epdr1*$^{-/-}$	Toronto Centre for Phenogenomics (TCP)	N/A
Mouse: wild-type C57Bl/6N	Toronto Centre for Phenogenomics (TCP)	N/A
Oligonucleotides		
TaqMan primers	Life Technologies	Table S5
SybrGreen primers	TAG Copenhagen	Table S5
Short interfering RNAs	Dharmacon	Table S5
Software and Algorithms		
Graphpad Prism 8.0 for statistical analysis	https://www.graphpad.com/	N/A
MaxQuant	https://maxquant.org/	Free
Perseus	http://www.coxdocs.org/doku.php?id=perseus:start	Free

LEAD CONTACT AND MATERIALS AVAILABILITY

Requests for reagents and resources should be directed to the Lead Contact, Camilla Scheele (cs@sund.ku.dk).

Disclosure of Limited Availability of Biological Material

We hereby disclose that the availability of biological material including the human cell cultures and tissue, is dependent on specific permission from the Danish Data Protection Agency and on the researcher's adherence to the specifications of this permission.

EXPERIMENTAL MODEL AND SUBJECT DETAILS

Human Supraclavicular (Brown) and Subcutaneous (White) Fat Precursor Cells

Brown fat precursor cells were isolated from the supraclavicular adipose depot of a cohort of adult humans (n = 21), as previously reported along with a subset of the cell cultures (Jespersen et al., 2013). These non-immortalized cell cultures were differentiated *in vitro* and the five cultures (from different individuals) displaying the best differentiation capacity in terms of lipid accumulation and the highest induction of UCP1 expression in response to norepinephrine (NE) were included in the study (Figure S1). The five brown fat precursor cultures were derived from two women and three men. White fat precursor cells were obtained from the subcutaneous abdominal region of three women and two men, with equal distribution of age and body mass index (BMI) as the donors of the brown fat cell cultures. All subjects provided written informed consent. The Scientific-Ethics Committees of the Capital Region and Copenhagen and Frederiksberg Municipalities Denmark approved the study protocols, journal numbers H-A-2009-020, H-A-2008-081, and (KF) 01-141/04, respectively, and the studies were performed in accordance with the Helsinki declaration.

Human Subjects

The human tissue and plasma samples used for this study are a subset from a cohort of subjects undergoing surgery for benign goiter. All subjects provided written informed consent prior to participation. The Scientific-Ethics Committees of the Capital Region of Denmark approved the study protocol and amendments, and the study was performed in accordance with the Helsinki declaration journal number H-1-2014-015. A subset of 30 non-obese normal glucose tolerant subjects were included in the current study. Surgical biopsies were obtained from the deep neck region and were snap-frozen in liquid nitrogen until RNA isolation was performed. Subject characteristics of EPDR1 positive and EPDR1 negative subjects are presented in Table S4.

Mouse Models

EPDR1 Injections

Animal studies were approved by the Animal Experimentation Inspectorate of the Danish Ministry of Justice no 2014-15-0201-00181. Mice were raised under Specific Pathogen Free (SPF) conditions. Acute injections: The animals were single housed and maintained at a 12-h light-dark cycle in temperature (30°C–32°C) and humidity (50–60%) controlled cabinets, with free access to standard chow (Altromin 1314F, pellets) and tap water. Chronic injections: The animals were maintained at a 12-h light-dark cycle in temperature (20°C–22°C) and humidity (50–60%) controlled cabinets, with free access to tap water and high fat diet (60 kJ% fat) from 6 weeks of age. At 22 weeks of age, the animals were single housed and placed in calorimetric chambers. Estimation of sample sizes were based on previous studies with similar metabolic readouts (Sustarsic et al., 2018).

Epdr1 *Knockout Mouse Model*

Animal studies were approved by the Toronto Centre for Phenogenomics Mt. Sinai Hospital, in Toronto. Mice were raised under SPF conditions. The mouse line C57BL/6N-Epdr1<tm1a(NCOM)Mfgc>/Tcp was generated at the Toronto Centre for Phenogenomics (TCP) and obtained from the Canadian Mouse Mutant. Repository as part of the NorCOMM2 project from NorCOMM ES cells (Bradley et al., 2012). Male mice generated from this mouseline were fed a regular standard rodent chow (18% kcal from fat, 2018 Harlan Teklad, Mississauga, ON) for 20 weeks. Epdr1-/- mice were gender and age matched to wild-type mice generated at the TCP facility that were not littermate controls.

METHOD DETAILS

Human Primary Adipocyte Culture Conditions

The protocols for isolation and differentiation of human fat precursor cells has been thoroughly described and discussed (Larsen et al., 2019). Cells were plated and maintained in DMEM F12 (Thermo Fisher Scientific) containing 10% FBS, 1% Penicillin/Streptomycin and 1nM FGF1 (Immunotools). Two days post confluence (designated day 0) the cells were induced to differentiate by replacing the medium with DMEM/F12 with 10 μg/ml Transferrin, 2 nM T3, 100 nM Insulin, 100 nM Dexamethasone, 200 nM Rosiglitazone and 540 μM 3-Isobutyl-1-methylxanthine (IBMX). At day 3, the medium was replaced with the same medium composition, with the exemption of IBMX. The cells were refed with new medium at day 6 and day 9 with the exemption of Rosiglitazone. At day 12, cells were considered fully differentiated mature adipocytes. Secretome analysis was performed on supraclavicular (n=5) and subcutaneous (n=5) cells. For secretome analysis, fully differentiated cells were washed with DMEM/F12 and subsequently incubated for 2 h in DMEM/F12 containing 1% penicillin-streptomycin. Serum-starved cells were stimulated with 10 μM norepinephrine (NE) (Sigma-Aldrich) for 4 h. Cell culture media (2 ml) was collected for secretome analysis while cells were harvested for RNA analysis. To address whether cell viability was affected by NE treatment, cells were stained according to the manufacturer's protocol, applying a LIVE/DEAD fluorescent assay (Thermo Scientific) visualized using an EVOS FL fluorescent microscope (Thermo Scientific).

siRNA Mediated Knockdown of EPDR1 in Adipocytes

At day 0 of the differentiation program, adipocytes were transfected with 22.2 nM siRNA targeting EPDR1 or a non-targeting pool (Dharmacon) (Table S5) using Lipofectamine RNAiMAX Reagent (Thermo Fisher Scientific) according to the manufacturer's instructions. The cells were then cultured as described in the previous section. To investigate whether our siRNA mediated knockdown of EPDR1 (using a pool targeting four different sites on the EPDR1 mRNA transcript and a non-targeting siRNA control) targeted the secreted isoforms of EPDR1 (transcript variant 1 and transcript variant 2), we designed qPCR primers specifically targeting either of these transcripts. A unique qPCR assay for the intracellular transcript variant 3 could not be designed, but a qPCR assay for assesment mRNA of all three transcript variants of EPDR1 was designed (Figures S4A–S4C; Table S5). To ensure that the knockdown was specific for *EPDR1* we also measured mRNA expression of *SFRP4*, which is located in the same locus as EPDR1, but transcribed from the opposite strand (Figure S4D). We validated the effects of EPDR1 knockdown on NE-induced thermogenic gene expression by transfecting with two additional siRNAs (Dharmacon) (Table S5), each targeting only one site of the mRNA molecule (Figure S2G). Finally, to investigate whether the observed reduction in induction of thermogenic gene expression following NE- stimulation in brown adipocytes following knockdown of *EPDR1* was specific for brown adipocytes, we also measured thermogenic gene expression in human white adipocytes (Figures S4E–S4G).

RNA Isolation and Quantitative Real-Time PCR of Adipocytes

Total RNA from human adipocytes was isolated with TRIzol (Thermo Fisher Scientific), according to the manufacturer's recommendations. RNA concentrations were measured using Nanodrop 1000, and 250 ng of RNA was used as input for subsequent cDNA synthesis with High Capacity cDNA Synthesis Kit (Thermo Fisher Scientific). Primer sequences can be found in Table S5. Target mRNA was normalized to PPIA and calculated using the comparative delta-delta-Ct method.

Oxygen Consumption Measurements in Adipocytes

Mitochondrial respiration rates were assessed using the XFe96 Extracellular Flux Analyzer (Agilent Technologies). Cells were plated at confluence (7000cells/well) and transfected and differentiated as described above. The cell medium was replaced with Seahorse Base medium without phenol red, supplemented with 1 μM L-Glutamine, 2 μM Na_2PO_4 and 25 mM Glucose pH 7.4 1 h prior to respiration measurements. Oxygen consumptions rates were followed under basal conditions, NE (1 μM) injection and finally oligomycin injection (20 μM).

Lipid and Mitochondrial Staining

Mature adipocytes were incubated with DMEM/F12 containing 0.2μM MitoTracker Red CMXRos (Thermo Fisher Scientific) for 20 min. Cells were then washed 3 times with PBS and fixed with 4% formaldehyde (Sigma-Aldrich) for 15 min. Fixed cells were washed again 3 times with PBS, and lipid were stained with 0.5 mM Bodipy (Thermo Fisher Scientific) for 20 min. Subsequently nuclei were stained with NucBlue Fixed ReadyProbe Reagent (Thermo Fisher Scientific) for 7 min. Cells were washed 3 times with PBS and visualized with EVOS FL imaging system (Thermo Fisher Scientific).

ELISA

EPDR1 Plasma concentrations were determined using a commercially available ELISA kit from Mybiosource. Briefly, 50 μl plasma were loaded in duplicates and EPDR1 abundance was determined. The detection limit of the kit was 30 ng/ml. UCP1 mRNA levels were determined using qPCR. Subject characteristics of EPDR1 positive and EPDR1 negative subjects are presented in Table S4.

EPDR1 Production

Production of recombinant human EPDR1 (UNIPROT entry Q9UM22, isoform 1, amino acids 39-224) was performed by transfecting expi293F cells growing in suspension culture in Expi293 Expression medium (ThermoFisher Scientific, cat# A1435101) with a mix of ExpiFectamine 293 Reagent (ExpiFectamine 293 Transfection Kit, ThermoFisher Scientific, cat# A14525) and plasmid DNA encoding the relevant sequence. Transfection Enhancers 1 and 2 from the ExpiFectamine 293 Transfection Kit were added the day after transfection. The cell culture was harvested 4 days after transfection. The recombinant EPDR1 secreted into the culture medium contained a short N-terminal sequence compatible with affinity purification and the protein was purified by affinity chromatography followed by size exclusion chromatography according to standard chromatographic methods. The purified protein solution was sterilized by filtration through a 0.2 mm filter unit.

Assessment of the Purity of EPDR1 Recombinant Protein

The purity of the protein was analyzed by SDS-PAGE. Briefly, Histidine tagged EPDR1 was loaded (6 μg) on SDS PAGE either directly or after three freeze thawing cycles (3 μg). The gel was stained with Coomassie blue stain (Figure S3A). A silver staining was also performed. Briefly, 2.92 ng and 3.18 ng protein from batch 2 and batch 3 was loaded on 4-12% Bis-Tris Nu PAGE gels (Thermo Fischer Scientific). Silver staining was done using SilverXpress, Silver staining kit (Thermo Fisher Scientific) and performed as recommended by the manufacturer (Figure S3A). The protein purity was also checked by using size exclusion chromatography (SEC) and protein identity was confirmed by LC MS-MS (Figure S3A). The protein solution was analyzed for endotoxin levels: batch 1: 0.059 EU/mg (used for indirect calorimetry study) and batch 2: 0.055 EU/mg (used for daily injections of EPDR1 over 21 days) batch 3: 0.68 EU/mg (used for [18F] FDG PET/CT imaging). All batches were confirmed to be suitable for animal studies. To further ensure that the observed increases in oxygen consumption following acute EPDR1 injection in C57BL/6NRj mice housed at thermoneutrality, was specific for EPDR1 and were not associated to artifacts coming from protein preparation, we measured metabolic parameters following injection of two other proteins. The two proteins (GM2A and SBSN) were also specifically quantified in the culture media from brown adipocytes and proteins were prepared/purified in the same manner as EPDR1. All further experimental conditions were also identical between setups (Figures S4H–S4K).

Small Animal [18F] FDG PET/CT Imaging

Eight-week-old female mice were group housed at thermo neutrality on a 12:12 hour light/dark cycle (lights on at 9 PM and off at 9 AM). [18F] FDG was administered intravenously between 10 AM and 2 PM. The average radioactive dose was 4.8 MBq (range: 3.6–5.8 MBq). EPDR1 (2 mg/kg) or PBS was administered subcutaneously 180 minutes prior to FDG injection, and CL 316,243 (1 mg/kg) or PBS was administered subcutaneously 15 min prior to FDG administration. Animals were fasted and housed in the dark at 29°C following injection of EPDR1.

Small animal PET/CT (Inveon Multimodality PET/CT scanner; Siemens) was performed 1 hour after FDG administration. Mice were anaesthetized by sevoflurane 40 minutes after FDG injection until the end of the imaging session. Heating was applied in order to maintain normal body temperature. PET data were acquired in list mode for 240s, and images were reconstructed using a 3-dimensional maximum a posteriori algorithm with CT-based attenuation and scatter correction. CT images were acquired using 360 projections, 65 kV, 500 mA, and 430 ms exposure and reconstructed with an isotropic voxel size of 0.210 mm. Images were analyzed using the Inveon software (Siemens). Quantitative analysis of the [18F]FDG uptake was performed by manually drawing region of interests over the areas containing iBAT based on the CT images. The FDG uptake was expressed as % injected dose per gram tissue (%ID/g). Animals were euthanized after the imaging session and iBAT, iWAT, Soleus muscle and heart were excised, weighted, submerged in RNAlater for subsequent RNA isolation and gene expression analysis.

RNA Isolation and Quantitative Real-Time PCR following EPDR1 Injection

Total RNA was extracted from iBAT and WAT depots that was stored in RNAlater. The tissues were processed in Tri Reagent (Qiagen) using a TissueLyser II system (Qiagen) and RNeasy Lipid Tissue Mini Kit according to instructions from the manufacturer. RNA concentrations were measured using Nanodrop 2000, and 500 ng of RNA was used as input for subsequent cDNA synthesis with High Capacity cDNA Synthesis Kit (Thermo Fisher Scientific). Primer sequences can be found in Table S5. Target mRNA was normalized to peptidylprolyl isomerase A (PPIA) and results were calculated using the comparative delta-delta-Ct method.

Indirect Calorimetry following EPDR1 Injection

Twelve-week (acute injections) or twenty-week (chronic injections) old male C57BL/6NRJ mice (Janvier Labs, France) were used for metabolic measurements. All animals were acclimatized in habituation cages one week before they were placed in the TSE phenomaster (TSE systems GmbH, Bad Homburg, Germany) system. Here they were acclimatized for another 4 days prior to the initiation of the injection experiments and measurements. Mice were randomized according in two groups of eight mice taking their weight into account. For the acute injection study, EPDR1 (2 mg/kg in PBS) or PBS as vehicle was administered subcutaneously 20 min prior to

the dark cycle. Metabolic measurements were followed for a total of 43 hours, and the initial 12-hour dark period was used to assess treatment effects. For the chronic injection study, EPDR1 (2 mg/kg in PBS) or PBS as vehicle was administered subcutaneously in the middle of the light cycle. Metabolic measurements were followed for a total of 21 days and used to assess treatment effects.

Body Composition, Food Intake and Indirect Calorimetry in EPDR1$^{-/-}$ Mice

Body composition was measured using Echo nuclear magnetic resonance system (Echo Medical Systems, Houston, TX) MRI, in the non-fasted state around 10 am at 20 weeks of age. Food intake was averaged over a 3-day period where mice were housed individually. To measure oxygen consumption (ml/hr), carbon dioxide production, respiratory exchange ratio, activity, and energy expenditure (kcal/hr) the Comprehensive Lab Animal Monitoring System (CLAMS; Columbus Instruments, Columbus OH) was used when mice were 9-11 weeks of age.

Ex Vivo Oxygen Consumption

iBAT was immediately harvested from non-fasted animals after CO2 euthanasia. iBAT was split into 3 depots of similar size (~10 mg of scaled weight) and kept at DMEM high-glucose media at 37°C. Tissues were then washed in filtered respiration buffer (PBS, 0.02% fatty acid free BSA, 25-mM glucose, 0.01% (vol/vol) of 100 mM Na pyruvate (Sigma)), minced with scissors, re-suspended in 1-ml respiration buffer and placed into a Mitocell chamber (MT200A, Strathkelvin Instruments, North Lanarkshire, Scotland) also kept at 37°C with a Clark electrode (Strathkelvin). Recordings were normalized to tissue scaled weight and each data point represents an average oxygen consumption from 3 depots from each animal.

RNA Isolation and Quantitative Real-Time PCR in EPDR1$^{-/-}$ Mice

Total RNA was extracted from iBAT that was harvested immediately from mice after CO2 euthanasia in the non-fasted state and stored at -80°C until processed in Tri Reagent (Molecular Research Center, Cincinnati, ON) using a TissueLyser II system (Qiagen, Germantown, MD). First strand cDNA was synthesized from DNase I-treated total RNA using the SuperScript III and random hexamers (Thermo Fisher Scientific, Markham, ON). Gene expression levels were quantified by real-time PCR using a QuantStudio System and TaqMan Gene Expression Master Mix and Assays (Thermo Fisher Scientific). Primer/probes were purchased from Thermo Fisher Scientific (Table S5). qPCR data were analyzed by 2-DeltaDeltaCt method, and expression levels for each gene were normalized to Tbp (TATA-box-binding protein).

Secretome Analysis by Mass Spectrometry

A high-resolution mass spectrometry (MS)-based approach was used to detect a highly complex secreted protein mixture from human primary brown and white adipose cell cultures. Serum free cell supernatants were trypsin digested, and the resulting peptide mixtures were directly analyzed in a single-run LC-MS format. We performed liquid chromatography with 2 h gradient and analyzed peptides on bench top quadrupole-Orbitrap instrument with very high sequencing speed and high mass accuracy in MS and MS/MS modes (Michalski et al., 2011). Label-free quantification of the MS data is performed in the MaxQuant environment while bioinformatics analysis was done with Perseus software (Tyanova et al., 2016).

Sample Preparation for Secretome and Cellular Proteome

Secretome analysis of the conditioned media from brown and white adipocytes was performed as described before (Deshmukh et al., 2015) with slight modifications. Proteins in conditioned media were denatured with 2 M urea in 10 mM HEPES pH 10 by ultrasonication on ice and acetone precipitated (overnight). Protein pellets were washed with 80% acetone and suspended in urea (6 M) and thiourea (2 M) buffer (pH 8). Proteins were reduced with 10 mM dithiothreitol for 40 min followed by alkylation with 55 mM iodoacetamide for 40 min in the dark. Proteins were digested with 0.5 μg LysC (Wako) for 3 h and digested with 0.5 μg trypsin for 16 h at room temperature. The digestion was stopped with 0.5% trifluoroacetic acid, 2% acetonitrile. Peptides were desalted on reversed phase C18 StageTips. The peptides were eluted using 20 μl of 60% acetonitrile in 0.5% acetic acid and concentrated in a SpeedVac. Concentrated peptides were acidified with 2% acetonitrile, 0.1% trifluoroacetic acid in 0.1% formic acid. Samples for cellular proteome of BAT and WAT cells were prepared according to iST protocol (Kulak et al., 2014).

LC MS/MS Analysis

The peptides from the cell culture media were analyzed using LC-MS instrumentation consisting of an Easy nanoflow UHPLC (Thermo Fischer Scientific) coupled via a nanoelectrospray ion source (Thermo Fischer Scientific) to a Q Exactive mass spectrometer (Thermo Fischer Scientific) (Michalski et al., 2011). Peptides were separated on a 50-cm column with 75-μm inner diameter packed in-house with ReproSil-Pur C18-aq 1.9 μm resin (Dr. Maisch). Peptides were loaded in buffer containing 0.5% formic acid and eluted with a 160 min linear gradient with buffer containing 80% acetonitrile and 0.5% formic acid (v/v) at 250 nL/min. Chromatography and column oven (Sonation GmbH) temperature were controlled and monitored in real time using SprayQC (Scheltema and Mann, 2012). Mass spectra were acquired using a data dependent Top8 method, with the automatic switch between MS and MS/MS. Mass spectra were acquired in the Orbitrap analyzer with a mass range of 300-1650 m/z and 70 000 resolution at m/z 200. HCD peptide fragments were acquired with a normalized collision energy of 25. The maximum ion injection times for the survey scan and the MS/MS scans were 20 and 220 ms, and the ion target values were set to 3e6 and 1e5, respectively. Data were acquired using Xcalibur software. Peptides from BAT and WAT cells were analyzed using LC-MS instrumentation consisting of an Easy nanoflow UHPLC

coupled via a nanoelectrospray ion source to a latest generaton Q Exactive mass spectrometer (HFX) (Kelstrup et al., 2018). Peptides were separated on a 50 cm column with 75 μm inner diameter packed in-house with ReproSil-Pur C18-aq 1.9 μm resin (Dr. Maisch). Peptides were loaded in buffer containing 0.5% formic acid and eluted with a 100 min linear gradient with buffer containing 80% acetonitrile and 0.5% formic acid (v/v) at 350 nL/min. Mass spectra were acquired using a data-dependent Top15 method, with the automatic switch between MS and MS/MS. Mass spectra were acquired in the Orbitrap analyzer with a mass range of 300-1650 m/z and 60 000 resolution at m/z 200. HCD peptide fragments were acquired with a normalized collision energy of 27. The maximum ion injection times for the survey scan and the MS/MS scans were 20 and 25 ms, and the ion target values were set to 3e6 and 1e5, respectively.

Computational MS Data Analysis

The raw files for secretome and cellular proteome were analyzed in the MaxQuant environment (Tyanova et al., 2016). The initial maximum allowed mass deviation was set to 6 ppm for monoisotopic precursor ions and 20 ppm for MS/MS peaks. Enzyme specificity was set to trypsin, defined as C-terminal to arginine and lysine excluding proline, and a maximum of two missed cleavages was allowed. A minimal peptide length of six amino acids was required. Carbamidomethylcysteine was set as a fixed modification, while N-terminal acetylation and methionine oxidation were set as variable modification. The spectra were searched by the Andromeda search engine against the human UniProt sequence database with 248 common contaminants and concatenated with the reversed versions of all sequences. The false discovery rate (FDR) was set to 1% for peptide and protein identifications. The peptide identifications across different LC-MS runs were matched by enabling the 'match between runs' feature in MaxQuant with a retention time window of 30 s. If the identified peptides were shared between two or more proteins, these were combined and reported in protein group. Contaminants and reverse identifications were removed from further data analysis. Protein quantification was based on the Max LFQ algorithm integrated into the MaxQuant software (Cox et al., 2014).

Bioinformatics analysis was performed with the Perseus software (Tyanova et al., 2016) (http://www.perseus-framework.org). Categorical annotation was supplied in the form of KEGG pathways, Keywords (UniProt), and Gene Ontology (GO) (biological process (BP), molecular function (MF) and cellular component (CC)). All annotations were extracted from the UniProt database. To define the secretome of brown and white adipocytes, we applied previously described computational workflow on all proteins identified in the media (Deshmukh et al., 2015). Briefly, signal peptide-containing proteins were categorized as 'classical' secreted proteins while protein annotated to 'extracellular location' (GOCC) or 'secreted' (UniProt, Keywords) were classified as 'non-classical' secreted proteins. While comparing proteins identified in the cell media from brown or white adipocytes with Vesiclepedia (Kalra et al., 2012) and ExoCarta databases(Keerthikumar et al., 2016), we included only evidence at the protein level.

The global comparative analysis was performed on LFQ intensities. We used very stringent criteria for MaxLFQ-based quantification (min ratio count 2 in MaxQuant). Moreover, we included only those proteins which were quantified at least 2 times in at least one group (i.e. Brown_woNE vs White_woNE) Due to the randomness of peptide sampling in shotgun proteomics, the quantification of several proteins is missing for some samples. The data was imputed to fill missing abundance values by drawing random numbers from a Gaussian distribution. These parameters have been tuned in order to simulate the distribution of low abundant proteins best. To investigate differences between brown and white adipocyte secretomes, we compared brown and white adipocyte media proteome under non-stimulated (woNE) conditions while the effect of NE-stimulation was investigated by comparing stimulated and non-stimulated conditions (Brown_woNE vs Brown_NE/ White_woNE vs White_NE). These comparisons were made using a two-sample t-test in Perseus with FDR 0.05. Proteins which were regulated by 1.5-fold (Log_2) were considered as significantly different proteins (Table S2). Two-sample t-test (volcano plot), hierarchical clustering and annotation enrichment were based on label-free quantitation of the samples. Hierarchical clustering of significantly different proteins was performed after Z-score normalization. We then performed Fisher exact test on significantly different proteins (background total quantified proteins), testing for enrichment or depletion of any annotation term in the cluster compared to the whole matrix.

Downstream analysis of global cellular proteome was performed in Perseus software. The statistical comparisons were made using a two-sample t-test in Perseus with FDR 0.05. Protein abundances were compared siCtr vs siEPDR1 in human brown adipocytes. While comparing siCtrl vs siEPDR1 in human brown adipocytes, proteins with >1.2 log_2 FC were considered as significantly differentially regulated.

Predictive Multiplexed Selective Ion Monitoring (pmSIM)

Predictive multiplexed selected ion monitoring (pmSIM) targeting in MaxQuantLive (version 1.0) for peptide and protein quantification relies on the real-time recalibration of retention time and mass accuracy based on background peptides and the identification of the heavy labeled counterpart of the to be quantified endogenous peptide of interest. Therefore, the heavy labeled EPDR1 peptide SYETWIGIYTVK was equally spiked into ready to inject brown and white fat secretomes and analyzed by data dependent acquisition on an orbitrap QE-HFX platform followed by MaxQuant (1.6.7) to identify retention time, intensity, and m/z of background peptides and the EPDR1 peptide SYETWIGIYTVK for pmSIM targeting of the endogenous counterpart. A total of 2743 shared realtime correction peptides were selected from the 'evidence' output file, removing potential contaminants, reverse database hits, modified sequences, miss cleaved peptides and peptides eluting in a time frame of <10 and >90min. For realtime correction, the initial retention time tolerance was ± 20 min and the final retention scale factor was set to three times the standard deviation of the recorded elution time with a mass tolerance of ± 9 ppm, and an intensity threshold of 10^{-5}. MaxQuant.Live pmSIM experiments of three biological replicates for brown (BAT5, BAT13, BAT19) and two for white fat (WAT11a, WAT13a) were performed with a 1st isolation window and a +0.2 Th

offset and acquired with a resolution of 120,000 at *m/z* 200. The heavy and light channels were multiplexed in a single scan. A maximum of 5 x 10^5 ions were collected in each channel with a maximum ion injection time of 120 ms for the light and heavy channel, respectively.

Data analysis of the pmSIM experiment was performed with the Skyline (Version 4.2.0.19009) and XCalibur (3.1.66.10) software suites. For data analysis light and heavy channel intensities for the EPDR1 peptide SYETWIGIYTVK were extracted from Skyline. Light channel intensities were normalized against the total background peptide MS1 intensity to take sample specific properties into account followed by normalization against the heavy channel. Fold change difference calculation was performed on the median white fat intensities.

Western Blot Analysis on Cell Media

For complement factor H, we validated proteomics data using western blot analysis on conditional media. The conditioned media was concentrated (3 different Brown adipocyte cell strains and 3 different White adipocyte cell strains) through two centrifugation rounds using an Amicon Ultra-4 3K and 10 K filter devices (Merk Millipore, USA). Purified proteins (FB Hycult HC2129, FH CompTech A137, FI CompTech A138) were used as positive control. Growth media was used as negative control. Precision Plus Protein Blue (Bio-Rad, USA) was used as molecular weight (MW) marker. The CFH antibody was produced in-house by Prof. Peter Garred's research group using mouse hybridomas and was used in a concentration of 1.8 μg/ml. The secondary antibody was Rabbit α-mouse HRP (Dako P0260 Lot# 00062101), utilized at a dilution of 1:10,000.

Western Blot Analysis on Cell Lysate

SiRNA mediated knockdown of EPDR1 was validated using western blot analysis on cell protein lysate. In short, the mature differentiated cells were washed twice with ice cold PBS and the lysed in lysis buffer containing 20 mM tris-HCl, 150 mM NaCl, 1 mM EDTA, 1 mM EGTA, 1% Triton-X, 2.5 mM $Na_4P_2O_7$, 1 mM β-glycerophosphate, 1mM Na_3VO_4, Complete Mini, Protease Inhibitor Cocktail. Lysates were centrifuged for 15 min at 13.000 g at 4°C. Protein concentration was determined using the Bio-Rad Protein (Bio-Rad, California, USA). 3.6 μg of protein lysate was loaded on Bis-Tris SDS-page gels and subject to electrophoresis, using iBright Prestained Protein ladder (Thermo Fisher Scientific) to determine MW of detected bands. Proteins were transferred to PVDF membranes by semi-dry transfer for 7 min with Pierce Power blot cassette. Membranes were blocked in FSG and incubated for 16 h with anti-EPDR1 at 1:1000 in 1% FSG (Thermo Fisher Scientific) or anti-α-Tubulin (Sigma-Aldrich) (1:1000 in 1% FSG). Bands were detected with IRDye secondary antibodies (LI-COR) at 1:5000 and visualized using the Odyssey Fc Imaging System (LI-COR).

QUANTIFICATION AND STATISTICAL ANALYSIS

Secretome data was collected from five separate brown adipocytes cultures derived from five different human donors and five separate white adipocytes cultures derived from five different human donors, thus representing biological replicates. Statistical analysis of proteomics data was performed using Perseus software (Tyanova et al., 2016). The details of the proteomics data analysis can be found in the STAR Methods in the section "Computational MS data analysis". Statistical analyses of the rest of the experiments were performed with GraphPad Prism software. No methods were used to further determine whether the data met assumptions of the statistical approach. For the cell experiments in Figures 3E and 3H–3J, a representative brown fat culture was utilized and technical replicates (n=3) from independent experiments are presented. To account for a putative batch to batch variation, effects of EPDR1 knockdown and norepinephrine was assessed using a Mixed-effects analysis in Graphpad Prism 8, using repeated measurements for both EPDR1 knockdown and norepinephrine analysis. In case of a significant overall effect of EPDR1 knockdown, specific effects were assessed with Sidaks multiple comparison's test for which p-values are presented in the graphs. In the interpretation of the qPCR data, it should be considered that no correction for multiple testing was performed. All 21 genes measured was reported. Genes assessed in the data set presented in Figure 3 that were not significantly regulated are presented in Figures S2I and S2J using the same statistical approach. Additional statistical details, including exact value, description and exclusion of n as well as definition of center, and dispersion and precision measures, are specified in the figure legends. A p-value below 0.05 was considered significant.

DATA AND CODE AVAILABILITY

The assession number for the mass spectrometry proteomics data reported in this paper is ProteomeXchange: PXD008541. The data have been deposited to the ProteomeXchange Consortium via the PRIDE (Perez-Riverol et al., 2019) partner repository.

Cell Metabolism, Volume *30*

Supplemental Information

Proteomics-Based Comparative Mapping of the Secretomes of Human Brown and White Adipocytes Reveals EPDR1 as a Novel Batokine

Atul S. Deshmukh, Lone Peijs, Jacqueline L. Beaudry, Naja Z. Jespersen, Carsten H. Nielsen, Tao Ma, Andreas D. Brunner, Therese J. Larsen, Rafael Bayarri-Olmos, Bhargav S. Prabhakar, Charlotte Helgstrand, Mai C.K. Severinsen, Birgitte Holst, Andreas Kjaer, Mads Tang-Christensen, Annika Sanfridson, Peter Garred, Gilbert G. Privé, Bente K. Pedersen, Zachary Gerhart-Hines, Søren Nielsen, Daniel J. Drucker, Matthias Mann, and Camilla Scheele

A

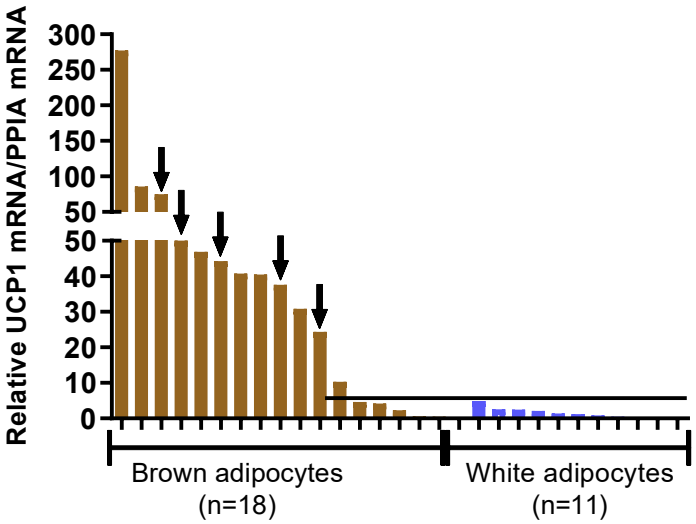
Relative UCP1 mRNA/PPIA mRNA
300
250
200
150
100
50
50
40
30
20
10
0
Brown adipocytes
(n=18)
White adipocytes
(n=11)

B

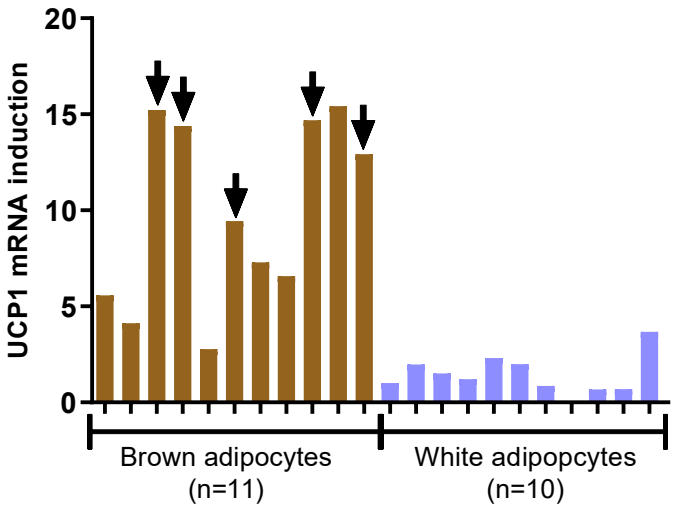
UCP1 mRNA induction
20
15
10
5
0
Brown adipocytes
(n=11)
White adipopcytes
(n=10)

C

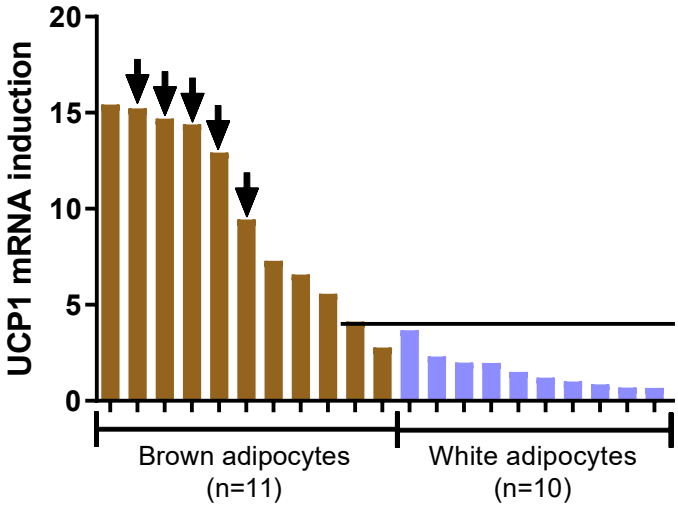
UCP1 mRNA induction
20
15
10
5
0
Brown adipocytes
(n=11)
White adipocytes
(n=10)

D

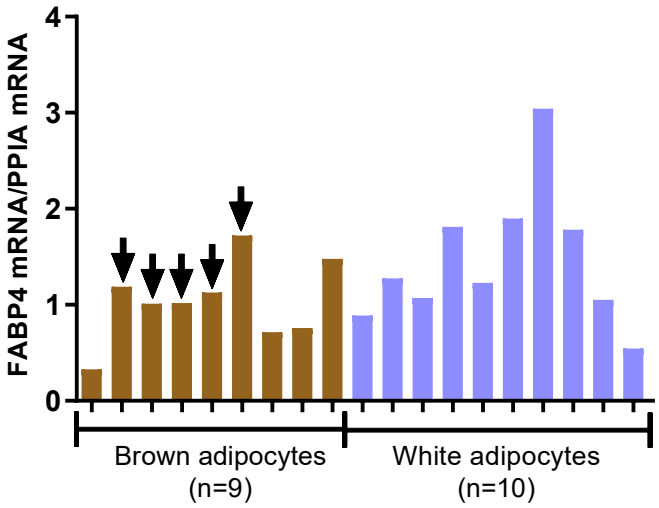
FABP4 mRNA/PPIA mRNA
4
3
2
1
0
Brown adipocytes
(n=9)
White adipocytes
(n=10)

E

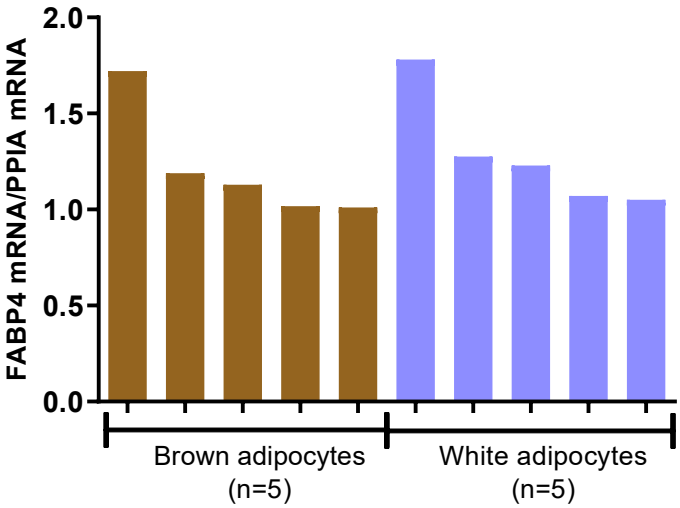
FABP4 mRNA/PPIA mRNA
2.0
1.5
1.0
0.5
0.0
Brown adipocytes
(n=5)
White adipocytes
(n=5)

Figure S1. Selection of cell cultures for secretomics experiment. Related to Figure 1.

Adipogenic precursor cells were isolated from the stromal vascular fraction of 21 biopsies obtained from the deep neck supraclavicular region (Jespersen et al., 2013). 18 of these cell cultures differentiated in vitro under the criteria of accumulating above 30% lipid droplets (as estimated using phase contrast microscopy). For comparison, we included white adipocytes derived from separate individuals while isolated and differentiated using the same protocols as used for the brown adipocytes. Prior to harvest, fully differentiated cells were stimulated for four hours with 10 µM norepinephrine (NE). The selected five brown adipocytes cultures are labelled black arrows throughout the graphs. **A)** Basal levels of *UCP1* mRNA was measured using qPCR and cell cultures were ordered after expression. Seven of the "brown" cultures overlapped with the "white" in terms of *UCP1* mRNA expression, while one "white" culture overlapped with the "brown". We therefore excluded these cultures, leaving us with 11 brown adipocyte cultures and 10 white adipocyte cultures **B)** Fold change of *UCP1* mRNA in response to NE, shown in the same order as in A. **C)** Fold change of *UCP1* mRNA in response to NE, ordered after *UCP1* mRNA induction. Two of the "brown" cultures overlapped in *UCP1* fold change with the "white" adipocyte cultures and were therefore excluded. **D)** FABP4 mRNA levels were measured using qPCR and cell cultures are ordered in the same order as in C. Cells with as high *UCP1* fold change and similar *FABP4* mRNA expression were selected, which is shown with black arrows **E)** *FABP4* mRNA levels in selected brown and white adipocytes. Data are relative gene expression levels for each individual sample, calculated using the delta delta CT method, using *PPIA* as an endogenous control.

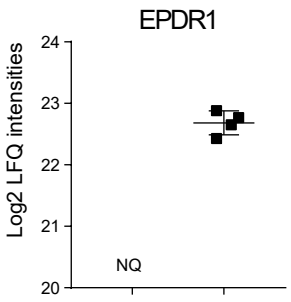

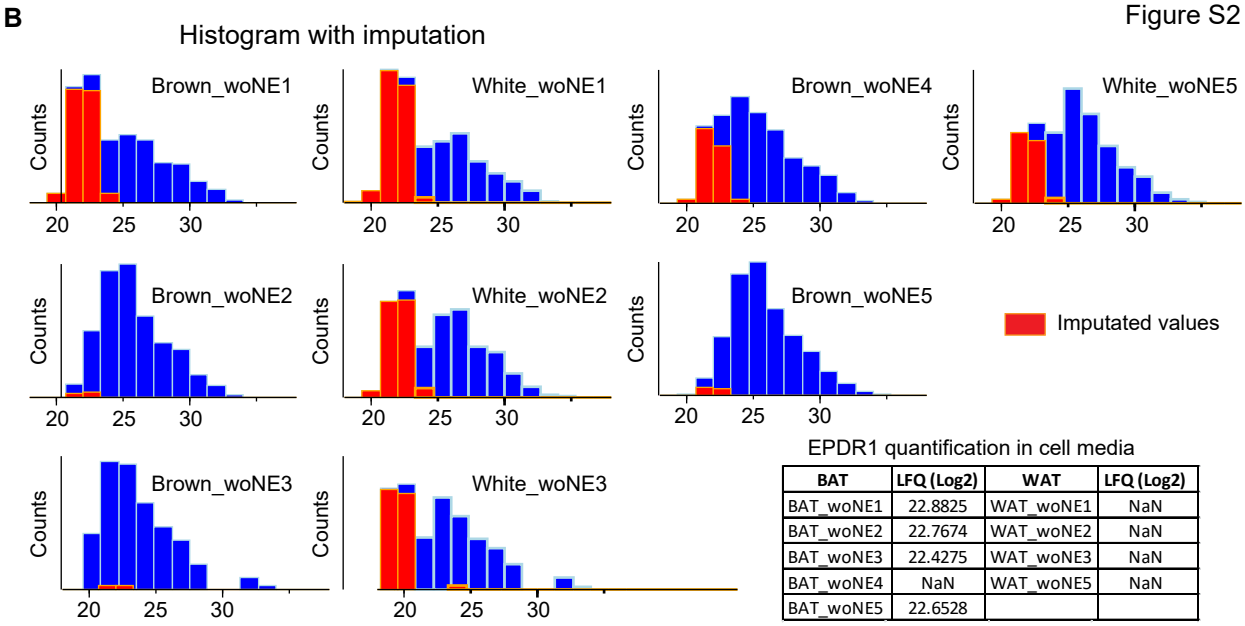

EPDR1 quantification in cell media

BAT	LFQ (Log2)	WAT	LFQ (Log2)
BAT_woNE1	22.8825	WAT_woNE1	NaN
BAT_woNE2	22.7674	WAT_woNE2	NaN
BAT_woNE3	22.4275	WAT_woNE3	NaN
BAT_woNE4	NaN	WAT_woNE5	NaN
BAT_woNE5	22.6528		

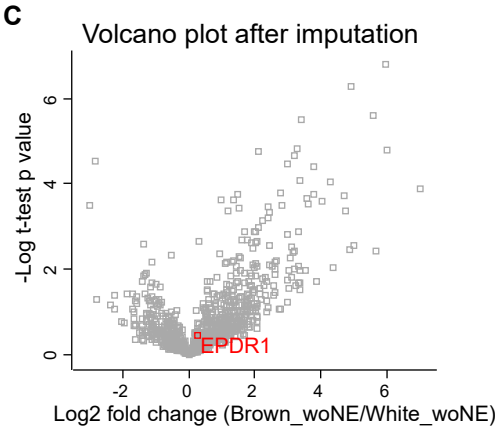

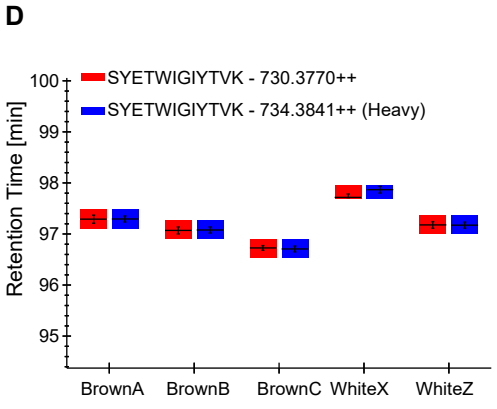

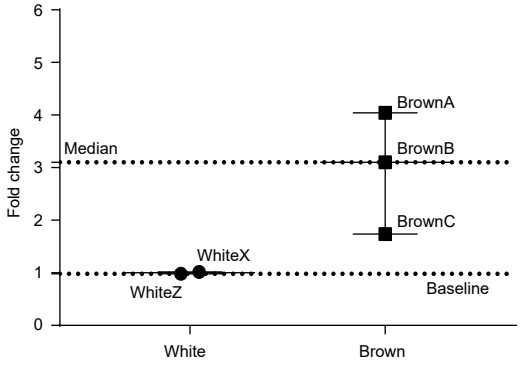

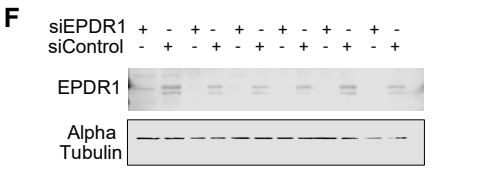

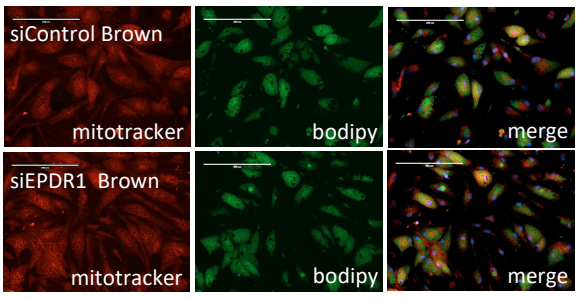

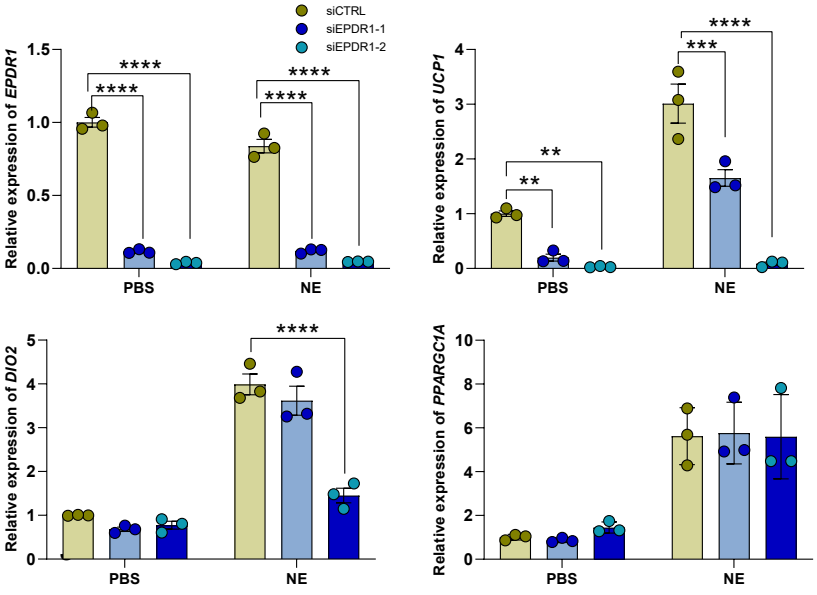

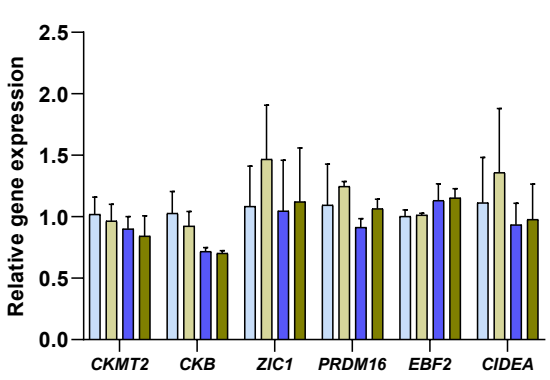

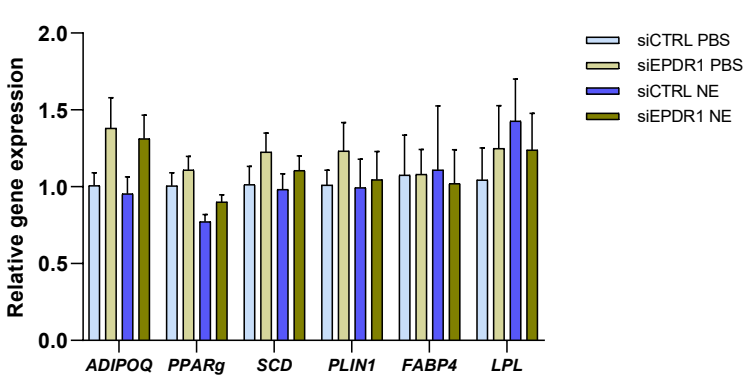

Figure S2. Identification and *in vitro* characterization of EPDR1. Related to Figure 3.

A) LFQ values of EPDR1 in white versus brown adipocytes **B)** Imputation histograms. **C)** Volcano plot with EPDR1 annotated. **D)** Skyline output of the co-eluting heavy labeled EPDR1 peptide standard and the corresponding endogenous one across the brown (n=3) and two white (n=2) biological replicates. **E)** Results of the EPDR1 derived peptide SYETWIGIYTVK predictive multiplexed Selected Ion Monitoring (pmSIM) targeting experiment in white (N = 2) and brown fat (N = 3). The fold change was in both cases normalized against the median white endogenous peptide expression level. Brown fat shows a median 3.1-fold higher expression level of EDPR1 than white fat. **F)** Western blot analysis of EPDR1 protein in white and brown adipocytes with or without siRNA knockdown of *EPDR1* (using a pool targeting four different sites of the *EPDR1* mRNA transcript and a non-targeting siRNA control). **G)** Gene expression analysis of thermogenic marker genes following transfection with two single-sequenced siRNAs targeting separate sites on the *EPDR1* mRNA transcript. A representative brown adipocyte culture was utilized and (n=3) represents three independent experiments. Data was analyzed using repeated measurements for siRNA transfection and norepinephrine stimulation and a Mixed effects analysis. In case of a significant ($P<0.05$) overall effect of EPDR1 knockdown, specific effects were assessed with Sidaks multiple comparison's test for which P values are presented in the graphs. Post-tests were performed comparing to the siRNA control samples. **H)** Representative image of mitochondrial (mitotracker) and lipid droplet (bodipy) staining in siEPDR1 or siControl transfected brown adipocytes (n=3). **I-J)** Relative gene expression of thermogenic and adipogenic marker genes unaltered following *EPDR1* knockdown. A representative brown adipocyte culture was transfected in n=3 independent experiments. Data are mean presented as +/- SEM; *P<0.05, **P<0.01, ***P<0.001, ****P<0.0001

A

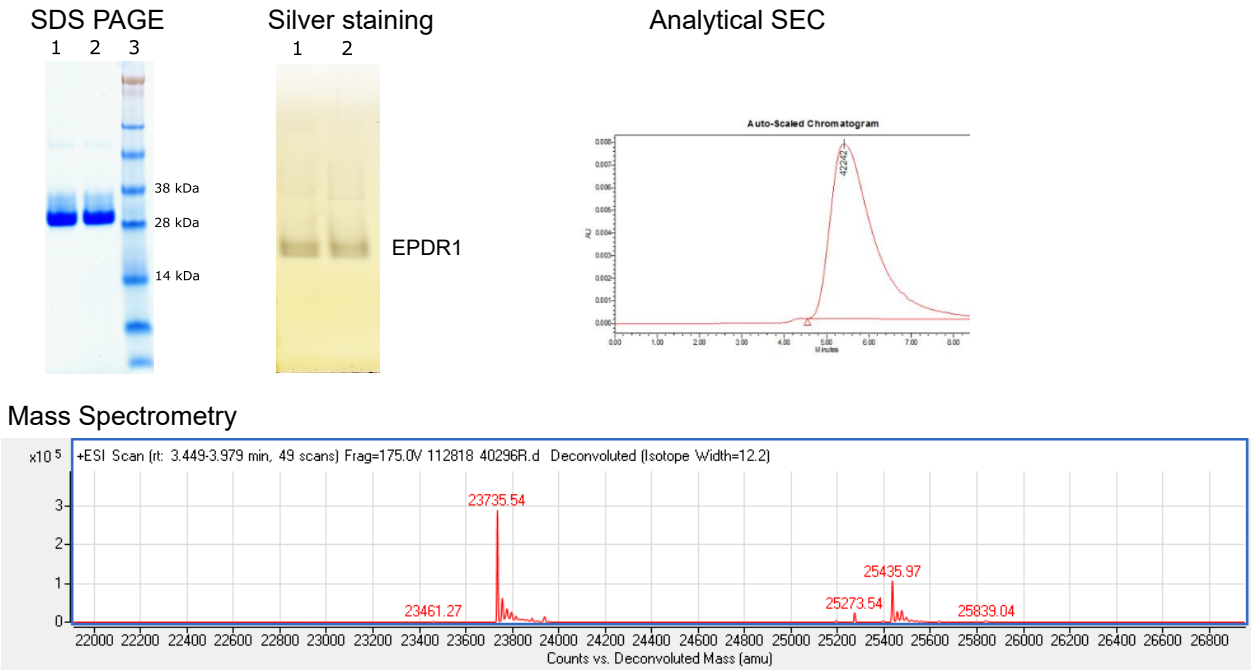
SDS PAGE
1 2 3
38 kDa
28 kDa
14 kDa
Silver staining
1 2
EPDR1
Analytical SEC
Auto-Scaled Chromatogram
Mass Spectrometry
+ESI Scan (rt: 3.449-3.979 min, 49 scans) Frag=175.0V 112818 40296R.d Deconvoluted (Isotope Width=12.2)
23735.54
23461.27
25435.97
25273.54
25839.04
Counts vs. Deconvoluted Mass (amu)

B

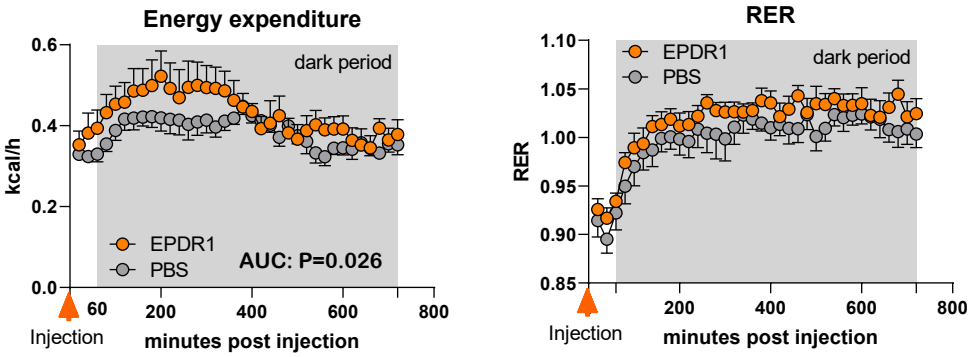
Energy expenditure
dark period
kcal/h
EPDR1
PBS
AUC: P=0.026
Injection
minutes post injection
RER
EPDR1
PBS
dark period
RER
Injection
minutes post injection

C

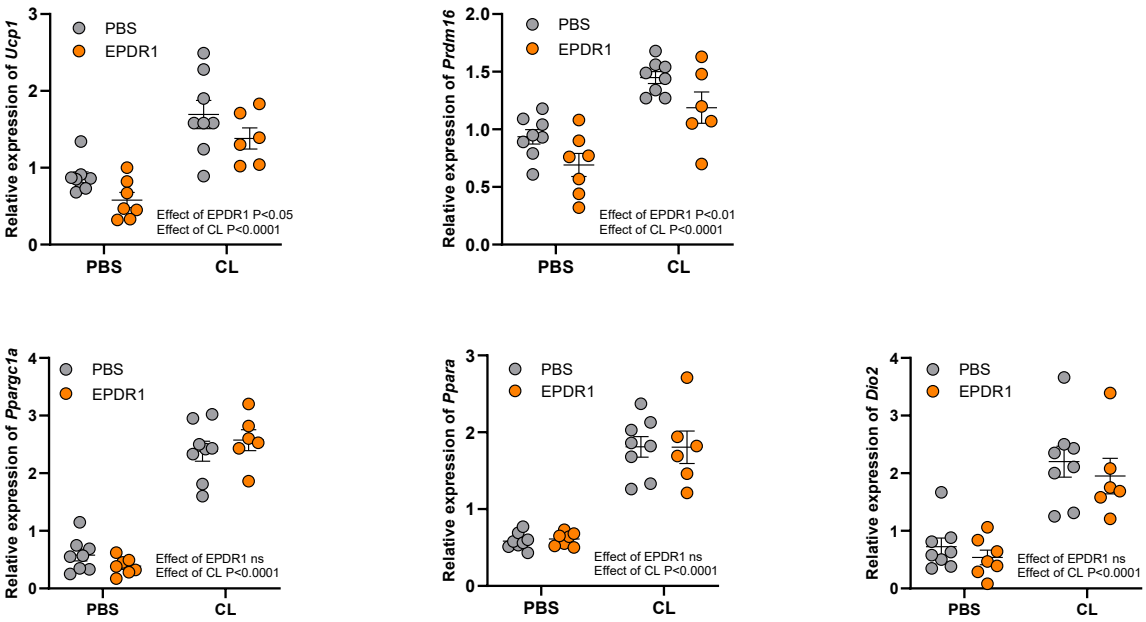
Relative expression of Ucp1
PBS
EPDR1
Effect of EPDR1 P<0.05
Effect of CL P<0.0001
PBS
CL
Relative expression of Prdm16
Effect of EPDR1 P<0.01
Effect of CL P<0.0001
Relative expression of Ppargc1a
Effect of EPDR1 ns
Effect of CL P<0.0001
Relative expression of Ppara
Effect of EPDR1 ns
Effect of CL P<0.0001
Relative expression of Dio2
Effect of EPDR1 ns
Effect of CL P<0.0001

D

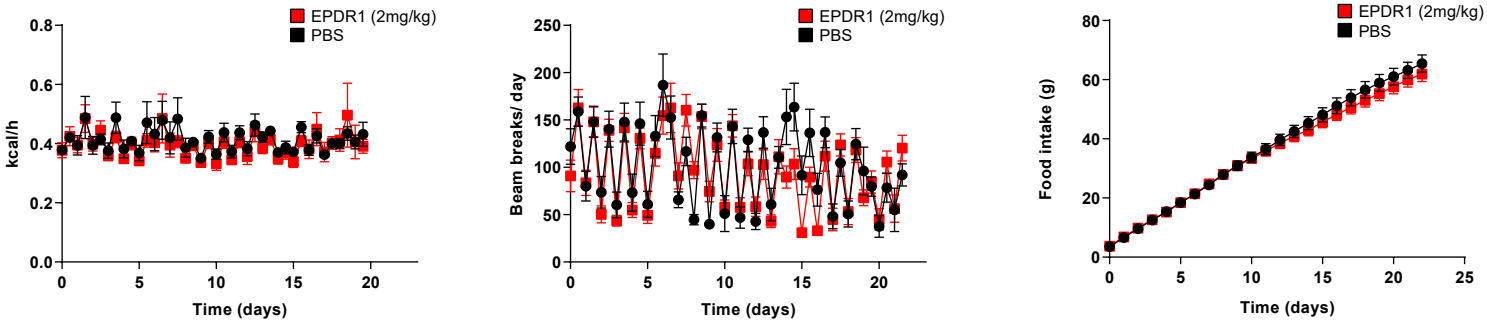
EPDR1 (2mg/kg)
PBS
kcal/h
Time (days)
Beam breaks/ day
Food intake (g)

Figure S3. Characterization and injections with human recombinant EPDR1. Related to Figure 4.

A) Coomassie blue staining of SDSPAGE, silver staining and liquid chromatography and mass spectrometry of EPDR1 isoform 1 protein. **B)** Calculated energy expenditure and Respiration Exchange Ratio (RER) following EPDR1 (n=8) or vehicle (n=8) injection in C57Bl/6NRj mice at thermoneutrality during the dark period. Unpaired t-tests of area under the curve (AUC) were performed to assess differences between groups. **C)** Relative mRNA expression of thermogenic markers *UCP1, PRDM16, PGC-1α, PPARα and DIO2* following injection of recombinant EPDR1 with and without injection of CL 316,243 in female C57Bl/6NRj mice at thermoneutrality and during FDG-PET/CT scanning at general anesthesia (n=6-8/group as one mouse in the EPDR1 injection group was euthanized due to a paralyzed leg, and two mice in the EPDR1 + CL injection group were excluded due to bad injections. A two-way Anova with no matching was performed to test the effects of CL and EPDR1 injections, respectively. **D)** Calculated energy expenditure, locomotor activity and food intake of C57/Bl/6NRj mice on HFD in room temperature following daily injections of EPDR1 or vehicle injections for 21 days (n=8/group). Data are presented as mean +/- SEM , p-value *<0.5**<0.01*** <0.001****<0.0001).

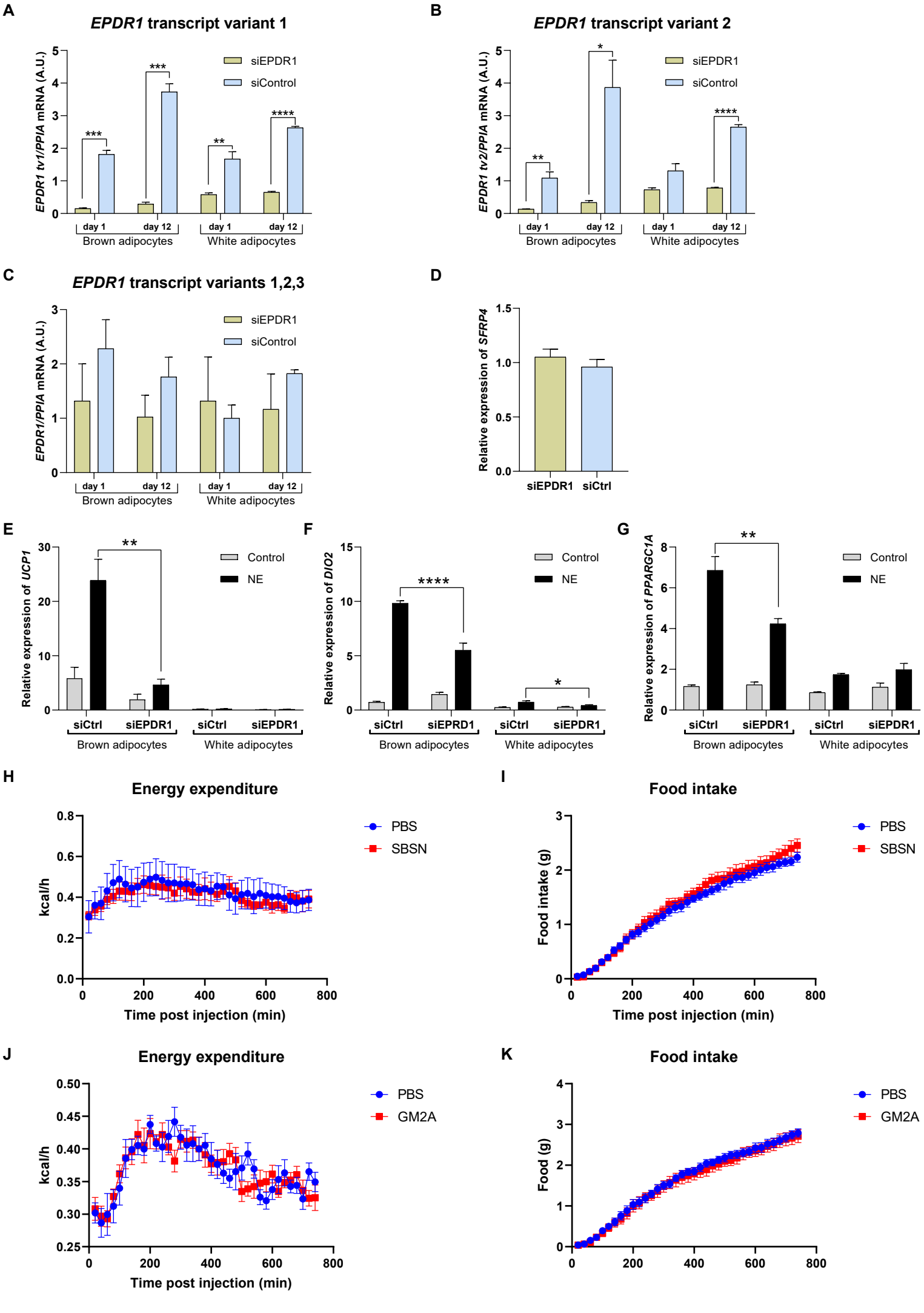
A
EPDR1 transcript variant 1
EPDR1 tv1/PPIA mRNA (A.U.)
siEPDR1
siControl
day 1
day 12
Brown adipocytes
White adipocytes
B
EPDR1 transcript variant 2
EPDR1 tv2/PPIA mRNA (A.U.)
C
EPDR1 transcript variants 1,2,3
EPDR1/PPIA mRNA (A.U.)
D
Relative expression of SFRP4
siEPDR1
siCtrl
E
Relative expression of UCP1
Control
NE
siCtrl
siEPDR1
F
Relative expression of DIO2
siEPRD1
G
Relative expression of PPARGC1A
H
Energy expenditure
kcal/h
PBS
SBSN
Time post injection (min)
I
Food intake
Food intake (g)
J
Energy expenditure
GM2A
K
Food intake
Food (g)

Figure S4. Validation of EPDR1 siRNA knockdown and EPDR1 recombinant protein. Related to STAR methods.

Transcription variant specific qPCR primers for *EPDR1* transcript 1 and 2, as well as a qPCR assay targeting transcript variant 1, 2 and 3 were designed and relative gene expression was measured to validate *EPDR1* siRNA knockdown was assessed **A)** Relative mRNA expression of *EPDR1* transcript variant 1 in white and brown adipocytes at day 1 and day 12 of differentiation following siRNA mediated knockdown of *EPDR1* at day 0. **B)** Relative mRNA expression of *EPDR1* transcript variant 2 in white and brown adipocytes at day 1 and day 12 of differentiation following siRNA mediated knockdown of *EPDR1* at day 0. **C)** Relative mRNA expression of all *EPDR1* transcript variants (1,2,3) in white and brown adipocytes at day 1 and day 12 of differentiation following siRNA mediated knockdown of *EPDR1* at day 0. **D)** Relative mRNA expression *SFRP4*, transcribed from the opposite DNA strand of *EPDR1* in brown adipocytes at day 12 of differentiation with or without siRNA knockdown of *EPDR1*. A-D were analyzed using paired t-tests to assess the effect of EPDR1 knockdown at each time point. **E)** Relative mRNA expression of *UCP1* in brown and white adipocytes with or without NE stimulation following knockdown of *EPDR1*. **F)** Relative mRNA expression of *DIO2* in brown and white adipocytes with or without NE stimulation following knockdown of *EPDR1*. **G)** Relative mRNA expression of *PPARGC1A* in brown and white adipocytes with or without NE stimulation following knockdown of *EPDR1*. E-G: Mixed effects analysis and Sidaks multiple comparison's test for which P-values are presented in the graphs. **H)** Calculated energy expenditure following injection of SBSN during the dark phase. **I)** Food intake following injection of SBSN during the dark phase. **J)** Calculated energy expenditure following injection of GM2a during the dark phase. **I)** Food intake following injection of GM2a during the dark phase. Data are mean +/- SEM; *P<0.05, **P<0.01, ***P<0.001.

Table S4. Human subject characteristics. Related to Figure 4A.

Group	Sex (F:M)	Age (years)	BMI (kg/m^2)	Fat%	P-EPDR1 (ng/ml)	UCP1 mRNA (A.U)
EPDR1-	6:1	56 (29 -74)	27 (20 – 38)	40.3 (25.9 – 50.8)	N.D.	31.9 (2.1 -11,416.8)
EPDR1+	17:6	48 (23 – 56)	30 (18 – 38)	38.7 (19.8 -54.1)	58.0 (34.7 - 213.8)	5724.5 (15.8 – 19,178.8)

Values are median and range. BMI = Body mass index, N.D. = not detectable

Table S5. Primers, probes and short interfering RNAs. Related to STAR Methods.

Gene	Taqman assay ID
hCFH	Hs00962373_m1
hCKB	Hs00176484_m1
hDIO2	Hs00255341_m1
hEBF-2	Hs00970588_m1
hPLIN1	Hs00160173_m1
hSFRP4	Hs00180066_m1
hUCP1	Hs01084772_m1
hZIC1	Hs00602749_m1
mDIO2	Mm00515664_m1
mEPDR1	Mm00840848_m1
mPGC1a	Mm00447183_m1
mPPARa	Mm00440939_m1
mPRDM16	Mm00712556_m1
mTBP	Mm00446973_m1
mUCP1	Mm01244861_m1

Gene	Forward primer (5'-3')	Reverse primer (5'-3')
hADIPOQ	CTGGTGAGAAGGGTGAGAAAG	GTTTCACCGATGTCTCCCTTAG
hCIDEA	TCAAGGGCCTGCTGAGGAGTCT	AAACTGTCCCGTCACCTGGGC
hCITED1	GAGGCCTGCACTTGATGTC	CACGGAGCTCATCTCTTGGT
hCKMT1	TGAGGAGACCTATGAGGTATTTGC	CTCATCAAAGTAGCCAGAACGG
hCKMT2	TGGTCGATCAGAGGTTGAGC	CTGTCGTACCAGCAGACAGAT
hCOL1A2	TCGCACATGCCGTGACTTG	GATAGCATCCATAGTGCATCCTTG
hEPDR1 tv1	GAGAGGAAGGCGCTGATCC	TGGCTTGGTCAATCTGAAACA
hEPDR1 tv2	TCTCCTACGACGGGCTCA	AGGTTTCATCTCTTGCAGGG
hEPDR1 all tv's	TGAAACCTGGATTGGCATCTATAC	TGTAGTTTATGGTAAAGGTTTCCTG
hFABP4	CCTTTAAAAATACTGAGATTTCCTTCA	GGACACCCCCATCTAAGGT
hGLUT4	CAATGGAGACGTAGCTCATGG	TGGCTGTGCCATCCTGATGAC
hLPL	TGCAGGAAGTCTGACCAATAAG	CCCTCTGGTGAATGTGTGTAAG
hPDGFRA	CGCGGTTTTTGAGCCCATTA	GCTCTGGGAAACTTCTCCTCC
hPGC-1a	CAAGCCAAACCAACAACTTTATCTCT	CACACTTAAGGTGCGTTCAATAGTC
hPPARa	GATGGAGACAGCTATGGTTTC	AAGTCAGTTTCGTTTGACCTG
hPPARg	AGCCTCATGAAGAGCCTTCCA	TCCGGAAGAAACCCTTGCA
hPPIA	ACGCCACCGCCGAGGAAAAC	TGCAAACAGCTCAAAGGAGACGC
hPRDM16	CACGAGTGCAAGGACTGC	TGTGGATGACCATGTGCTG
hSCD	TCTTCTCTCACGTGGGTTGG	AGCCAGGTTTGTAGTACCTCCT
mDIO2	GCTTCCTCCTAGATGCCTACAA	AGTCAAGAAGGTGGCATTCG
mPGC1a	CACTTCAATCCACCCAGAAAGCT	GGACATGTGCAGCCAAGACTCT
mPPARa	TGGTGTTCGCAGCTGTTTTG	AGATACGCCCAAATGCACCA
mPPIA	GGGTTCCTCCTTTCACAGAA	GATGCCAGGACCTGTATGCT
mPRDM16	CCTGTGGGAGTCCTGAAAGA	CAGCTTCTCCGTCATGGTTT
mUCP1	GGATTGGCCTCTACGACTCA	TAAGCCGGCTGAGATCTTGT

Short interferring RNAs	Assay Id
Non-targeting Pool	D-001810-10
hEPDR1 (pool of 4)	L-013378-01
hEPDR1 (Individual)	J-013378-09
hEPDR1 (Individual)	J-013378-10